AD-A091 721 TRW DEFENSE AND SPACE SYSTEMS GROUP REDONDO BEACH CA F/G 7/4
MONTE CARLO SIMULATION OF NEGATIVE ION COLLECTION BY A ROCKET-B--ETC(U)
JUN 80 T SUBIMURA, R D MCGREGOR F19628-77-C-0020
UNCLASSIFIED AFGL-TR-80-0206 NL

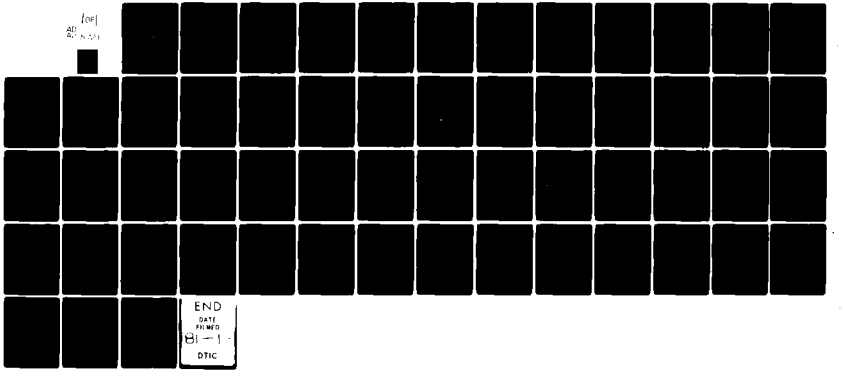

AFGL-TR-80-0206

MONTE CARLO SIMULATION OF NEGATIVE ION COLLECTION BY A ROCKET-BORNE MASS SPECTROMETER

by

Takashi Sugimura and R. D. McGregor

TRW Defense and Space Systems Group
One Space Park
Redondo Beach, California 90278

Final Report
Jan 77 — Dec 79

Jun 80

F19628-77-C-0020

2310

G3

Approved for Public Release;
Distribution Unlimited

Prepared for

AIR FORCE GEOPHYSICS LABORATORY
AIR FORCE SYSTEMS COMMAND
UNITED STATES AIR FORCE
HANSCOM AFB, MASSACHUSETTS 01731

UNCLASSIFIED

SECURITY CLASSIFICATION OF THIS PAGE *(When Data Entered)*

REPORT DOCUMENTATION PAGE	READ INSTRUCTIONS BEFORE COMPLETING FORM
1. REPORT NUMBER: AFGL-TR-80-0206 — 2. GOVT ACCESSION NO.: AD-A091 721	3. RECIPIENT'S CATALOG NUMBER
4. TITLE *(and Subtitle)*: MONTE CARLO SIMULATION OF NEGATIVE ION COLLECTION BY A ROCKET-BORNE MASS SPECTROMETER	5. TYPE OF REPORT & PERIOD COVERED: Final Report 1/77 through 12/79
	6. PERFORMING ORG. REPORT NUMBER
7. AUTHOR(s): R. D. McGregor, Takashi Sugimura	8. CONTRACT OR GRANT NUMBER(s): F19628-77-C-0020
9. PERFORMING ORGANIZATION NAME AND ADDRESS: TRW Systems Group, One Space Park, Redondo Beach, CA 90278	10. PROGRAM ELEMENT, PROJECT, TASK AREA & WORK UNIT NUMBERS: 61102F, 2310G3AC
11. CONTROLLING OFFICE NAME AND ADDRESS: Air Force Geophysics Laboratory, Hanscom AFB, Mass. 91731, Contract Monitor: C. Sherman/LKD	12. REPORT DATE: June 1980
	13. NUMBER OF PAGES: 55
14. MONITORING AGENCY NAME & ADDRESS *(if different from Controlling Office)*	15. SECURITY CLASS. *(of this report)*: unclassified
	15a. DECLASSIFICATION DOWNGRADING SCHEDULE

16. DISTRIBUTION STATEMENT *(of this Report)*

Approved for public release; distribution unlimited.

17. DISTRIBUTION STATEMENT *(of the abstract entered in Block 20, if different from Report)*

18. SUPPLEMENTARY NOTES

19. KEY WORDS *(Continue on reverse side if necessary and identify by block number)*

Monte Carlo	Debye length
Ion flux	Plasma sheath
Free molecule flow	Rocket-Borne probes
Transistional regime	Ionoshperic chemistry

20. ABSTRACT *(Continue on reverse side if necessary and identify by block number)*

The direct simulation Monte Carlo method developed for the prediction of positive ion collection by a rocket-borne probe has to be extended to simulate negative ion collection. It is found that realistic probe potentials can produce a high stagnation-point flux of negative ions while completely rejecting positive ions. However, this flux of negative ions is strongly attenuated by collisions at finite Knudsen numbers.

Additionally, the necessary theory has been developed so that direct simulation of nonequilibrium chemistry in the ionsphere can be performed.

DD FORM 1 JAN 73 1473 EDITION OF 1 NOV 65 IS OBSOLETE

UNCLASSIFIED

SECURITY CLASSIFICATION OF THIS PAGE *(When Data Entered)*

TABLE OF CONTENTS

LIST OF FIGURES

LIST OF FIGURES (CONT.)

ACKNOWLEDGEMENT

The authors wish to thank C. Sherman of AFGL and G. A. Bird from the Universtiy of Sydney, Australia for helpful suggestions concerning this study.

NOMENCLATURE

A_D	collecting disc area
$C_I = \frac{N_i}{n_{i_\infty} u_\infty A_D}$	ion flux coefficient
D	diameter
E	electric field
e	charge on electron
K	mobility
k	Boltzmann's constant
m	mass
m*	reduced mass
N	number density
p	pressure
Q	collision cross section
$S = u_\infty \sqrt{\frac{2kT_\infty}{m}}$	speed ratio
T	temperature
U	velocity
$\overline{V} = \sqrt{\frac{2kT}{m}}$	thermal velocity
V_d	drift velocity
$\alpha =$	r_o/r_e
$\gamma =$	ϕ_o/ϕ_e
λ_∞	mean free path
λ_D	Debye length
μ	polarizability

NOMENCLATURE (CONT.)

σ	particle diameter
ϕ	electric potential

Subscripts

∞	free steam conditions
e	electron
i	ion

1. INTRODUCTION AND SUMMARY

The objective of contract number F19628-77-C-0020 has been to establish a connection between the properties of the ambient ionosphere and the strength and chemical state of the flux entering a rocket-borne mass spectrometer. More specifically, the primary concern of this study was the description of the collection of negative ions by a flat-faced cylinder, approximately 15 cm. in diameter, travelling through a weakly ionized gas. The approach taken was to use the Direct Simulation Monte Carlo Method originated by G. A. Bird. This method was developed initially for neutral gases and has been extended to a plasma in the presence of a charged body with a consistent electric field. Since the electric potential distribution requires a solution of Poisson's equation the charged particle calculations require an iterative procedure between the Monte Carlo results and a finite difference solution of Poisson's equation. This approach was successfully developed and applied under previous contracts to predict the collection of positive ions. The results of these calculations along with the details of the direct simulation Monte Carlo procedure are presented in Vogenitz (1973), Sugimura and Vogenitz (1973,1975), and Sugimura (1976).

In the present study, the computer code developed for positive ion collection has been modified to predict the flux of negative ions to a rocket-borne mass spectrometer. The technical approach and formulation of the problem is outlined in Section 2. The interaction between ions and neutral atoms is addressed in Section 3. Section 4 presents a parametric variation of applied potential, Debye length, and Knudsen number on the flux of negative ions. Section 5 investigates the simulation of ionospheric chemistry as a collision process and includes the effects of internal degrees of freedom. Finally, the conclusions are presented in Section 6 where it is noted that the influence of angle of attack was not investigated due to the excessive computational requirements associated with the 3-dimensional flowfield and electric field.

2. TECHNICAL APPROACH

2.1 PROBLEM FORMULATION

In the present study, the negative ion flux to a rocket borne mass spectrometer is investigated. The collection of negative ions requires a positive collecting potential on the front face. This positive potential, however, also attracts the electrons which will reduce the collecting potential and the effectiveness of the instrument. The sampling of negative ions requires a circular double disk configuration; Sherman and Parker (1970), on the front face to repel the electrons while still collecting negative ions. The geometry and the potential distribution along the front face of the instrument payload will be approximated as shown in Figure 1. Although the face potential, Φ_o, would be greater than the mask potential, Φ_e, the mask has greater area. Therefore, only the proper ratio of Φ_o, to Φ_e, will allow the ions to pass through the collecting orifice for a given set of free stream and boundary conditions.

The most important assumption of the Monte Carlo simulation regards the treatment of the electrons. For the positive ion collection, the front face is negatively charged which repels the electrons and attracts the positive ions. The negative front face potential was assumed large enough so that the electrons could be taken to be in equilibrium with the local potential and determined by the Boltzmann distribution

$$\frac{N_e}{N_{e\infty}} = e^{(e\phi/kT_e)} \qquad (1)$$

where

N_e = electron number density

$N_{e\infty}$ = free steam value

ϕ = electric potential

T_e = electron temperature

e = charge on electron

This assumption was shown by Vogenitz (1973) to be accurate and was then used throughout the previous studies. The great simplification of this assumption

was that the electron trajectories could be ignored and only the ion motion was computed with the only coupling between the ion and electron distributions occurring through the electric potential determined from Poisson's equation

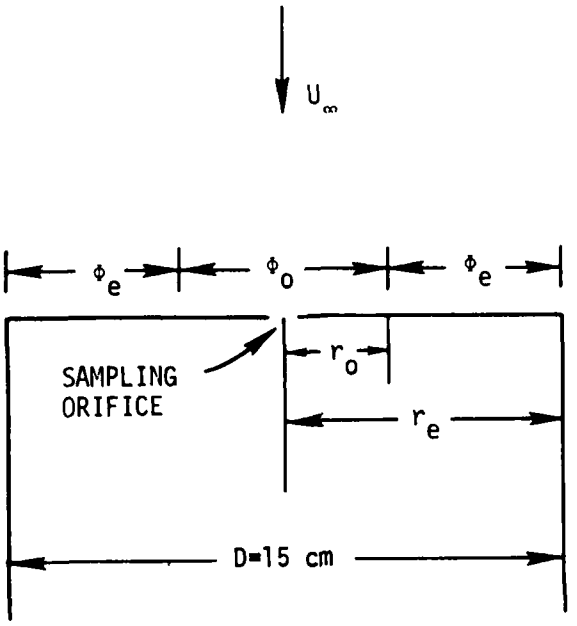

Φ_c = positive collection potential for negative ion
Φ_e = negative electron mask potential

Figure 1. Front Face Geometry

$$\nabla^2\Phi = \left(\frac{\lambda_\infty}{\lambda_D}\right)^2 (\bar{N}_i^+ - \bar{N}_e) \qquad (2)$$

where

$\Phi = \frac{e\phi}{kT_\infty}$ = non-dimensional electric potential

λ_∞ = mean free path

λ_D = Debye length

$\bar{N}_i^+ = \frac{N_i^+}{N_{i\infty}}$ = positive ion number density ratio

$\bar{N}_e = \frac{N^e}{N_{e\infty}}$ = electron number density ratio

For the collection of negative ions, this equilibrium assumption for the electrons is not rigorously justified. However, it was necessary to make this same assumption since the process of explicitly simulating electron trajectories was found to involve prohibitive computational complexity. This complexity arises for three reasons: (1) significant additional memory is required to store the coordinates and velocity components of the electrons; (2) the high thermal speed of the electrons necessitates a much smaller time step in the simulation which results in a large increase in computation time; (3) the explicit simulation of electron trajectories allows for greater statistical fluctuations of local charge densities thereby decreasing the stability of the iterative process for determining an ion flowfield with a consistent electric field. It should be noted that this assumption has no effect on the calculations for large Debye numbers since, in that case, the electric field is not significantly affected by the ion-electron distribution. For smaller Debye numbers, the results of the simulation appear to be realistic and hence it was concluded that the approximation did not produce a significant adverse effect.

For the collection of negative ions, two hypotheses regarding ion concentrations are appropriate. The first of these is the same as was made in the problem of positive-ion collection, namely, the gas is weakly ionized and hence the ions and electrons are trace species compared to the neutral atoms. Thus, the flow of the charged species is affected by the neutrals, but not vice versa. Additionally, the interaction of charged particles occurs only through the electric field, not through binary encounters. The second hypothesis is that the concentration of negative ions is small compared to that of positive ions. The literature on ionospheric composition indicates that this is indeed the case under the great majority of conditions. The benefit of this hypothesis can be seen by noting that the Poisson equation appropriate for the general problem of negative ion collection is given by

$$\nabla^2\Phi = \left(\frac{\lambda_\infty}{\lambda_D}\right)^2 (\bar{N}_i^+ - \bar{N}_i^- - \bar{N}_e) \qquad (3)$$

where all the variables are identical to those defined in Equation (2) with addition of

$$\bar{N}_i^- = \frac{N_i^-}{N_{i\infty}} = \text{negative ion number density ratio}$$

If the concentration of negative ions is negligible, then the term involving $\bar{N}_i^-$ can be dropped and hence the calculation of the negative-ion flux to the cylinder face reduces to a process of allowing the negative ions to percolate through the neutral-molecule flowfield with a fixed electric field determined solely by the positive ions and electrons. This computational procedure for the negative-ion sampling is outlined more fully in the following section.

2.2 COMPUTATIONAL PROCEDURE

The calculation procedure for the collection of negative ions is shown in the flowchart of Figure 2. It consists of the following steps:

(1) Initialize the problem by specifying the geometry and flow conditions, e.g.,

- Vehicle velocity
- Mean free path for neutral molecules
- Debye lenth
- Electric potential distribution on the vehicle.

(2) Since the ions and electrons are trace species, the neutral molecule flowfield can be determined without considering the ions and electrons. The neutral flowfield computed by the Monte Carlo direct simulation method is used as a scattering field for the ion and electron distributions. This calculation is performed only once for a given mean free path and can be used for all Debye lengths. In the collisionless limit, this calculation is bypassed.

(3) At this point, the ion and electron number densities have not been determined. Therefore, the first iteration for the electric potential is found by solving the Laplace equation

$$\nabla^2 \Phi = 0 \qquad (4)$$

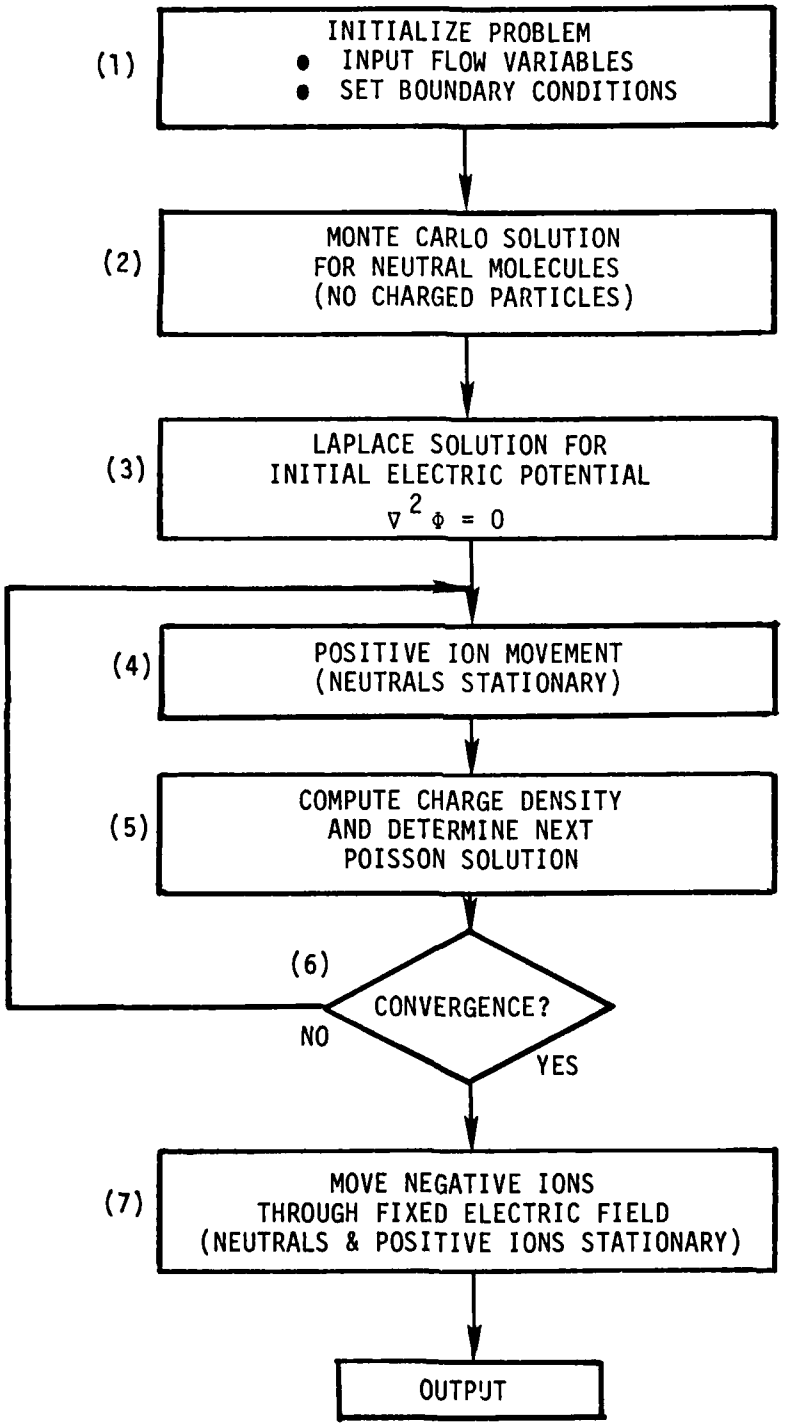

FIGURE 2. Flow Chart for Negative Ion Collection

If the Debye length is infinite (i.e., $\lambda_D = \infty$), this potential is exact and no further solutions of the Poisson equation are needed.

(4) The neutrals are kept stationary while the motion of the positive ions (appropriate to a small time interval) is computed using the present electric potential distribution.

(5) The new charge density and corresponding electric potential is calculated for the current distribution of electrons and positive ions.

(6) Convergence of the electron and positive ion distributions for a consistent Poisson solution is assessed. This is accomplished by checking the charged particle distributions for the current results with the previous iteration to see if steady state has been reached. If not, the iteration continues by returning to step (4).

(7) With the neutrals and positive ions held stationary, the negative ions are moved repeatedly in the fixed electric field to determine the flux to the instrument face.

It should be noted that step (4) requires an understanding of the interaction between positive ions and neutrals. Additionally, an understanding of electron-neutral interactions is needed if the electron motion were to be directly simulated. This subject of charged particle-neutral interaction is discussed in the next chapter.

3. CHARGED PARTICLE-NEUTRAL INTERACTION

Monte Carlo calculations performed for the electron motion in a neutral gas at densities where collisions are important indicated that the drift velocities were much higher than accepted measured values. After confirming the correctness of the numerical procedure, the basic assumptions for the simulation were reexamined.

In the past simple hard spheres were used for the charged particle-neutral scattering model and the collision cross section was computed from

$$Q_{pn} = \pi\left(\frac{\sigma_p + \sigma_n}{2}\right)^2$$

where σ_p = charged particle diameter

σ_n = neutral particle diameter

For the ions (p = i)

$$Q_{i_n} = \pi\left(\frac{\sigma_i + \sigma_n}{2}\right)^2 \tilde{=} \pi\sigma_n^2 \quad (\sigma_i \tilde{=} \sigma_n)$$

and for the electrons (p = e)

$$Q_{en} = \pi\left(\frac{\sigma_e + \sigma_n}{2}\right)^2 \tilde{=} \pi\frac{\sigma_n^2}{4} \quad (\sigma_e << \sigma_n)$$

The simple hard sphere model used for convenience in the earlier studies was justified on the basis that the gross features of the ion collection process were not clearly understood and in the collection of positive ions the electron trajectories were not computed. However, the present task of simulating the collection of negative ions requires accurate calculations of the electron motion.

The proper description of the charged particle-neutral encounter can be represented by an interaction potential of the form

$$V(r) = Ae^{-\beta r} + \sum_{n=4} C_n r^{-n}$$

where the first term represents strong, short range repulsive forces due to ordinary neutral particle gas kinetics and the succeeding terms represent attractive forces which arise between the charged particle and the polarized structure of the neutral.

In the calculations presented here a 4^{th} power attraction suggested originally by Langevin was used. The attractive force, due to polarization of the neutral molecule is given by

$$F = \frac{2\mu e^2}{r^5}$$

where μ = polarizability

e = electronic charge

The current Monte Carlo calculations treat the charged particle-neutral encounter as a binary collison involving both attractive and repulsive forces. The particle trajectories due to the repulsive force can be separated into two effects: (1) isotropic scattering at an impact parameter inversely proportional to the relative velocity of the collision, (2) isotropic scattering by a hard sphere core of fixed radius. The dominance of (1), (2) or the attractive force depends on the value of the impact parameter. For low energy encounters the attractive force would dominate, whereas for high energy encounters strong repulsive forces would be most important (see Figure 3).

The collision diameter σ_o for the attractive force is found to be

$$\sigma_o = 2r_o = 2\left(\frac{4e^2\mu}{m^* u_r^2}\right)^{1/4}$$

where $m^* = \frac{m_p m_n}{m_p + m_n}$

u_r = relative velocity of the encounter

This diameter can be compared to the standard hard sphere diameter σ_n to illustrate the polarization effect. For example, oxygen has a polarizability

$$\mu \simeq 1.6 \times 10^{-24} \text{ cm}^3$$

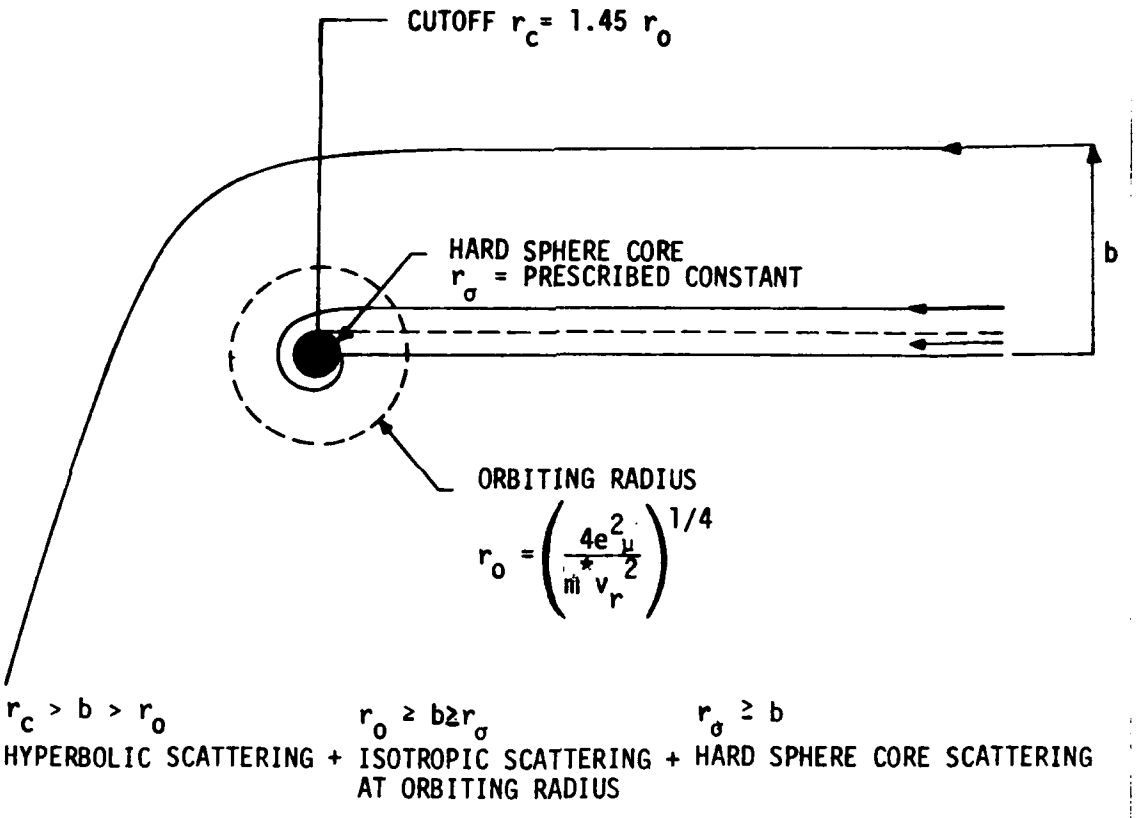

Figure 3. Charged-Neutral Scattering Model

and a hard sphere diameter

$$\sigma_n \tilde{=} 3 \times 10^{-8} \text{ cm}$$

The reduced mass for the ion-neutral interaction becomes

$$m^* = \frac{m_n m_i}{m_i + m_n} \tilde{=} \frac{m_n}{2} \quad (m_i \tilde{=} m_n)$$

At 300°K the relative velocity can be approximated by

$$u_r^2 \tilde{=} \frac{2kT}{m} = 1.4 \times 10^9 \ \frac{cm^2}{s^2}$$

Finally the ratio of the diameters is found to be

$$\frac{\sigma_o}{\sigma_n} \tilde{=} 5.3$$

This result implies that the collision cross section for oxygen ion-neutral encounters at 300°K is approximately 25 times the typical hard sphere value.

To investigate the results of this collision model a simple relaxation process has been studied. Consider a weakly ionized gas composed of electrons, positive ions and neutral particles which are initially in equilibrium at a single temperature. The positive ions are singly charged and of mass equal to the neutral particles. A prescribed constant electric field is instantaneously applied and subsequently maintained and the molecular motion of the gas is computed in time as a steady state is approached. The physical situation to which this corresponds could be imagined to consist of a gas contained between parallel electrodes of unlimited extent and great separation. Attention is focused upon a thin slab of this gas within which the spatial gradients can be ignored. Since all charged-charged interactions are contained in the electric field, which is known and constant for this case, the electron and ion motions are independent. Only the encounters of the charged particles with the neutral particles while under the influence of the electric

field determine the behavior of the charged particles.

Quantities of interest for this study are the following:

1) the steady state drift velocity per unit field, e.g. the mobility
2) the relaxation times
3) the temperature and shape of the distribution function in the steady state

In the ion collection process by a rocket borne mass spectrometer biased at a potential ϕ the parameter $e\phi/kT$ is used to characterize the strength of the electric field. In the present example of a gas contained between parallel electrodes the parameter E/P, field strength over neutral gas pressure, is used. The acceleration of a particle with charge e and mass m in an electric field E is eE/m. The energy acquired by the particle from the field between collisions is approximately $eE\cdot\lambda$ where λ is the mean free path. Since λ is inversely proportional to the density

$$E\cdot\lambda \sim E\cdot\frac{1}{\rho} \sim \frac{E}{P}\cdot T$$

or

$$\frac{E\lambda}{T} \sim \frac{E}{P}$$

Therefore the ratio of the field energy to thermal energy is proportional to E/P. This result assumes the field strength is low and that the masses of the ion and neutral particle do not differ greatly (thus excluding electrons). For arbitrary field strength and ion mass, E/P is less useful. However, most experimental data are presented in terms of it.

Results of computations made with this model is shown in Figures 4 through 7. Here the product of the mobility $K = V_d/E$ where V_d = drift velocity, E = electric field and the pressure, p, in atmospheres is shown for the electrons in a neutral gas with molecular weight 29. The calculations compare adequately with the experiments which have been influenced by effects not modeled in the simulation such as charge transfer, quantum mechanical resonance effects and clustering.

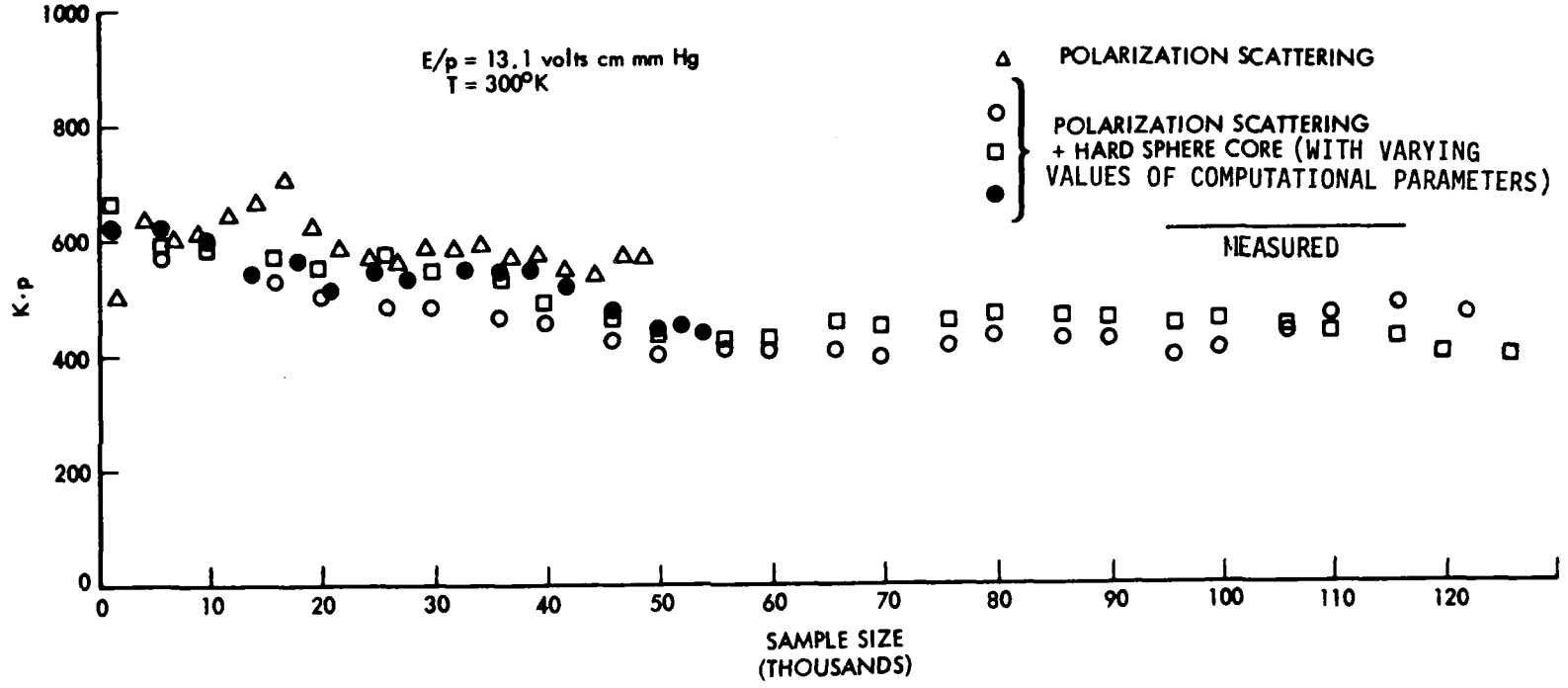

Figure 4. Electron Mobility

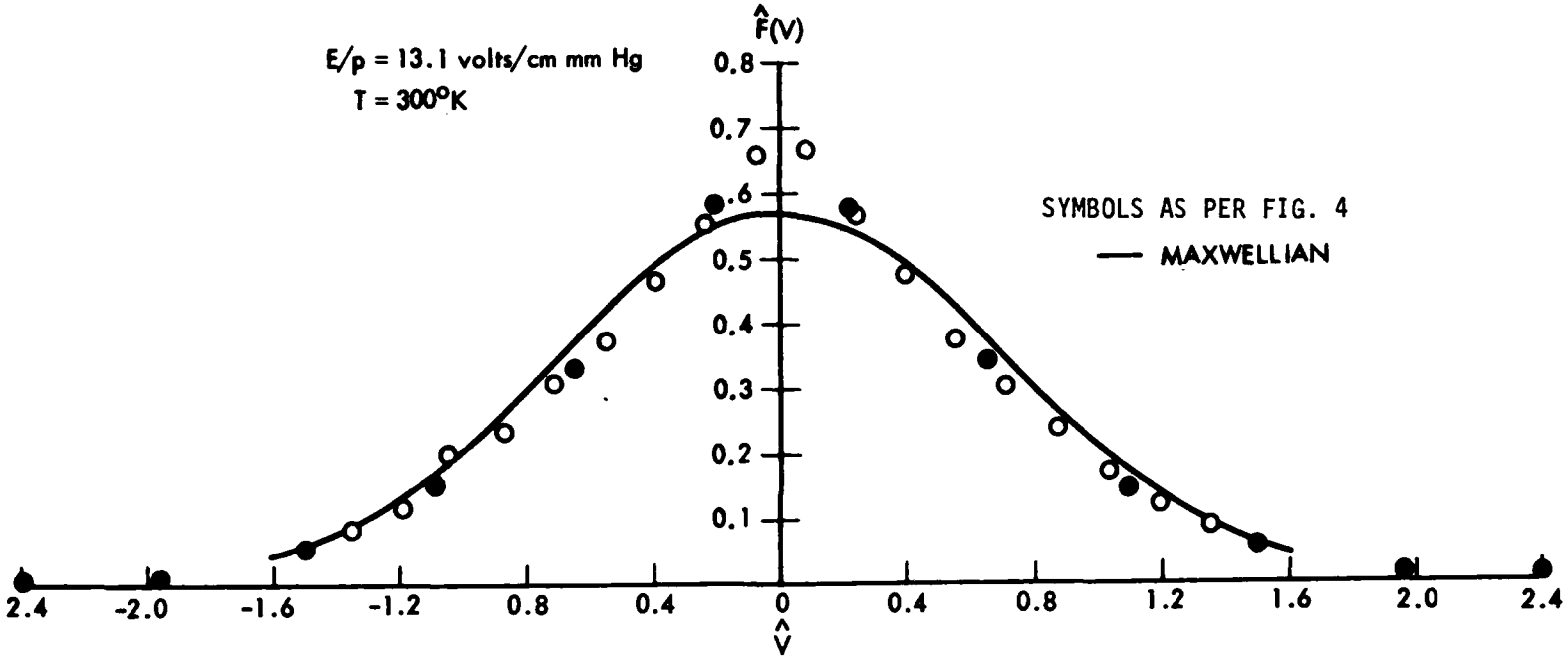

Figure 5. Electron Velocity Distribution

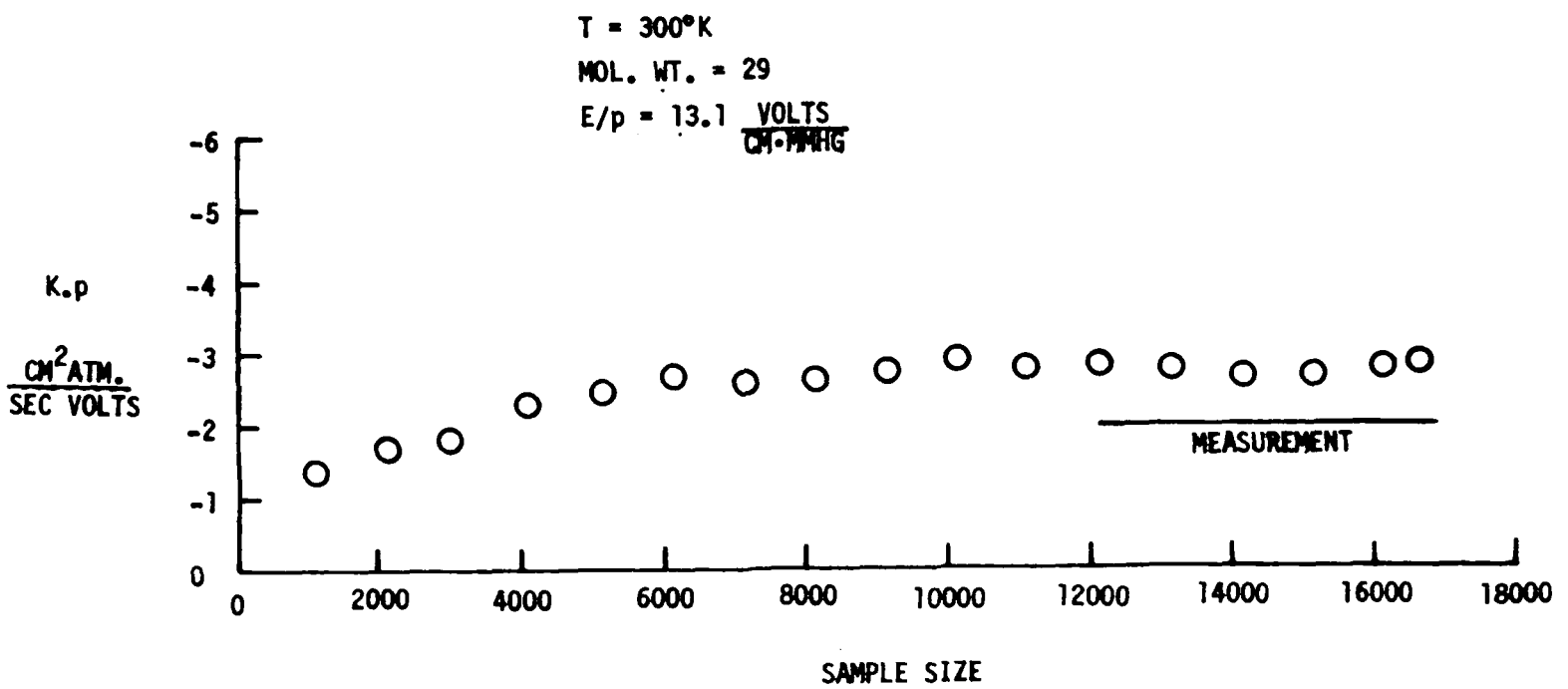

Figure 6. Ion Mobility

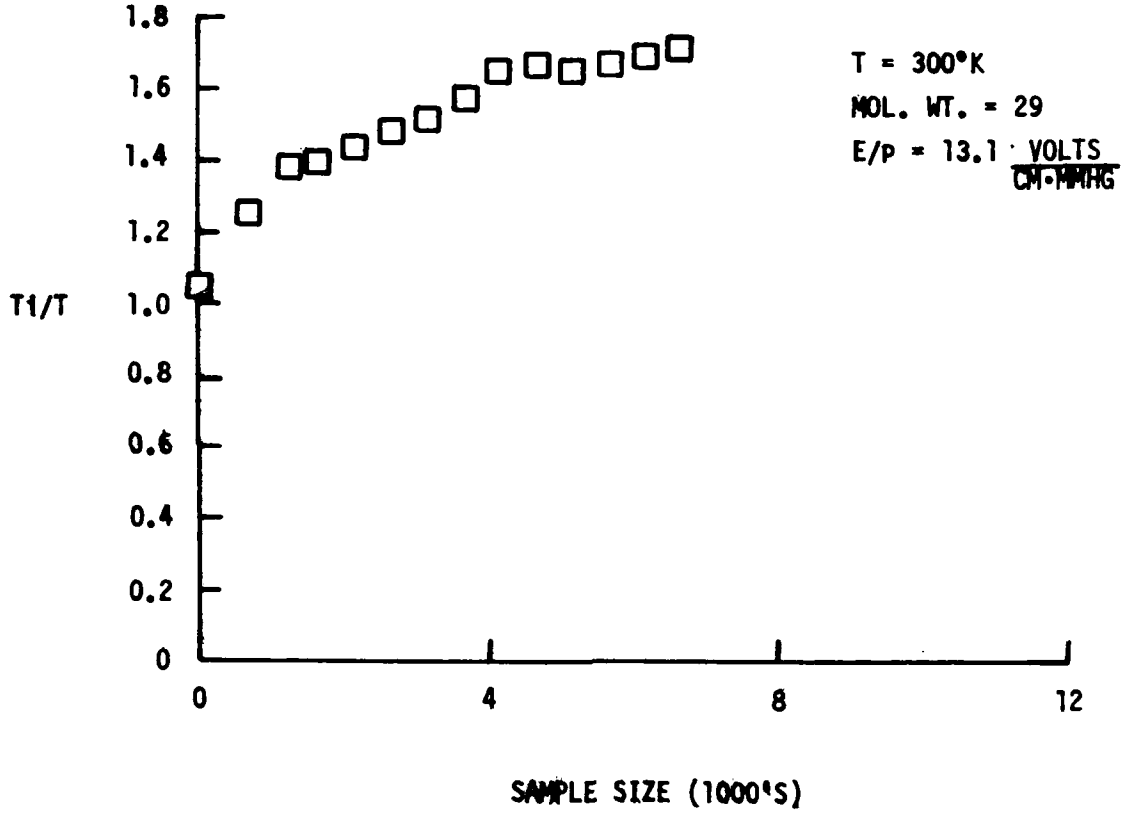

Figure 7. Ion Temperature Convergence

4. NEGATIVE-ION COLLECTION RESULTS

4.1 COLLISIONLESS, INFINITE DEBYE NUMBER RESULTS

A series of calculations have been performed to predict the collection of negative ions to the probe geometry shown in Figure 1 for the case in which both the Knudsen number and Debye number are infinite. The primary purpose of these calculations was to investigate the effects of the ratio of positive (Φ_o) to negative (Φ_e) front face potential. The fact that the Debye number is infinite is not as restrictive as might be imagined since it was found that (just as in the case of positive-ion collection) the Laplace solution was valid for Debye numbers as small as 1.0. The Laplace solution for the double-disk geometry was given by Sherman and Parker (1970) and can be characterized by the following parameters:

$$\text{ratio of disk radii, } \alpha = r_o/r_e$$

$$\text{ratio of potentials, } \gamma = \Phi_o/\Phi_e$$

Since the attracting potential, Φ_o, is positive and the electron mask is negative, it is possible that the potential along the stagnation line can become negative and repel the negative ions. Sherman and Parker show that the critical value of γ is given by

$$-\gamma_c = \frac{\sqrt{1 - \alpha^2}}{1 - \sqrt{1-\alpha^2}}$$

where this variation is shown in Figure 8. If $|\gamma| < |\gamma_c|$ there is a repelling potential along some portion of the stagnation line, while for $|\gamma| > |\gamma_c|$ the potential along the stagnation line is always positive.

Calculations were made for γ slightly larger and slightly less than the critical value for several values of α. The purpose of this series of calculations was to investigate the sensitivity of negative ion collection to variations in the potential ratio. The other parameters were as follows:

$$\text{Knudsen number } \frac{\lambda^\infty}{D} = 1000 \text{ (free molecule flow)}$$

$$\text{Debye number } \frac{\lambda D}{D} = 1000 \text{ (Laplace solution)}$$

$$\text{Speed ratio } S = 3.1$$

$$\text{Stagnation potential } \Phi_o = 200$$

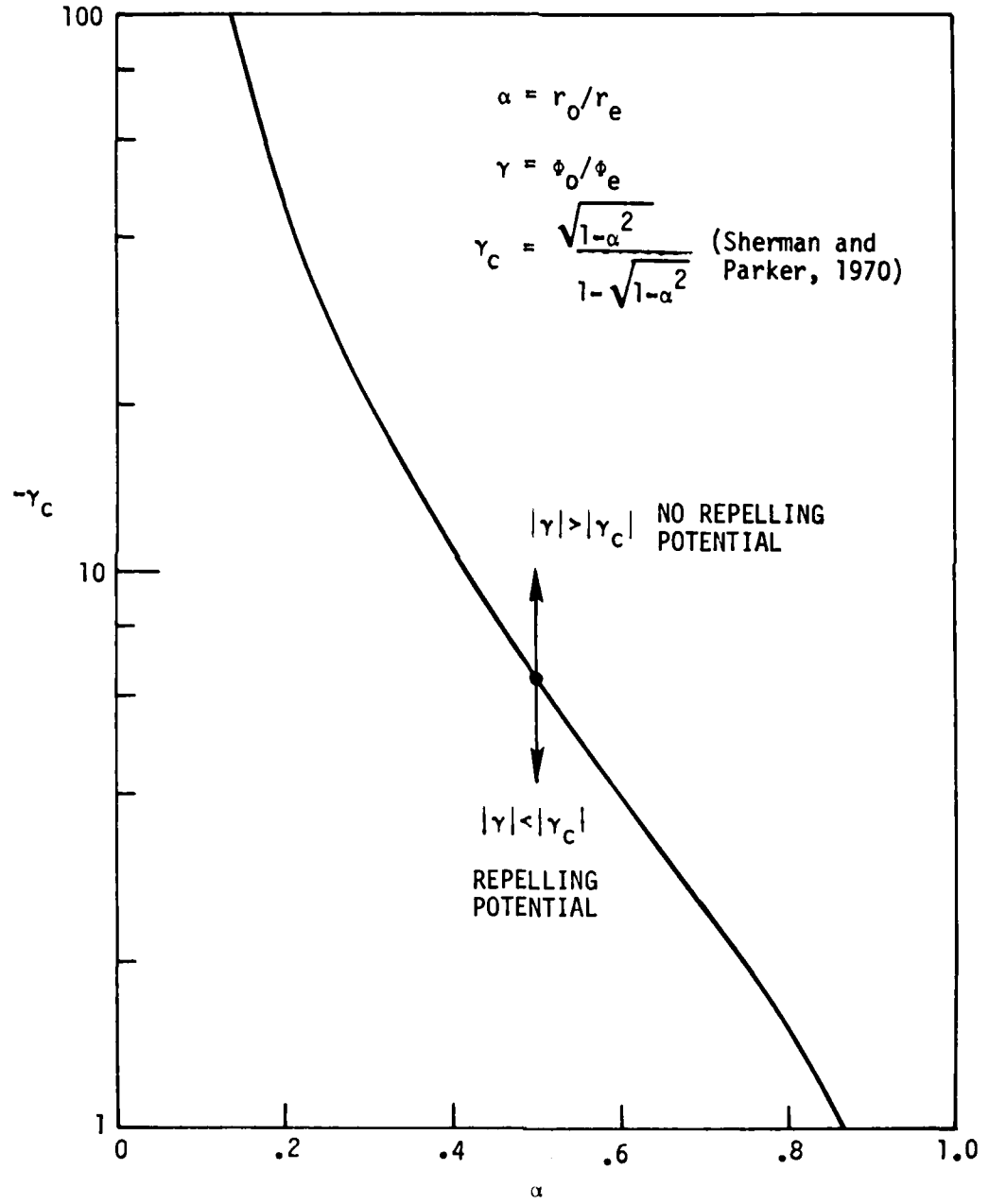

FIGURE 8. Critical Potential Ratio

An example of these calculations is given in Figure 9. The result was that moderate changes in repelling potential have only a small effect on the ion flux. In terms of electron shielding, however, the smaller values (in magnitude) of potential ratio are more desireable. As a balance between these two considerations, it appeared reasonable to choose $\alpha = 0.5$, $\gamma = -5$ (yielding a small repelling potential) for the subsequent calculations investigating the effects of finite Knudsen and Debye numbers. The choice of $\alpha = 0.5$ (with a commensurate value of γ) is motivated by the results shown in Figure 10 where it can be seen that this choice achieves close to the maximum stagnation-point ion flux yet still provides a reasonably sized electron mask.

4.2 FLUX VARIATION WITH KNUDSEN NUMBER

The simulations for various Knudsen numbers were performed with the values of the other parameters set as previously specified. (It should be noted that in all the results reported in this work, the sidewall potential was assumed to be zero.) For finite Knudsen numbers, the cross-section for ion-neutral and collisions becomes relevant. In the present results, the ion-neutral and neutral-neutral cross-sections were assumed to be equal. [Although this assumption is not correct, it serves to provide Knudsen number variation at minimum computational expense. If an absolute flux is desired, then an accurate estimate should be obtained by basing the Knudsen number on the ion-neutral mean free path, rather than the neutral-neutral mean free path. From this point of view, we have effectively increased the neutral-neutral mean free path to equal the ion-neutral mean free path (rather than vice versa) with the resultant effect of reducing neutral flowfield gradients which are limited anyway by cell dimensions.] The variation of the stagnation-point ion flux coefficient as a function of Knudsen number is shown in Figure 11. It shows that the effect of collisions becomes significant starting at a Knudsen number of order 10. This conclusion is shown more directly in Figure 12 by plotting the percentage of the total ion flux contributed by freestream ions (i.e., those ions that have not been affected by the body either directly through collisions with the body or indirectly through collisions with other molecules that have been affected by the body).

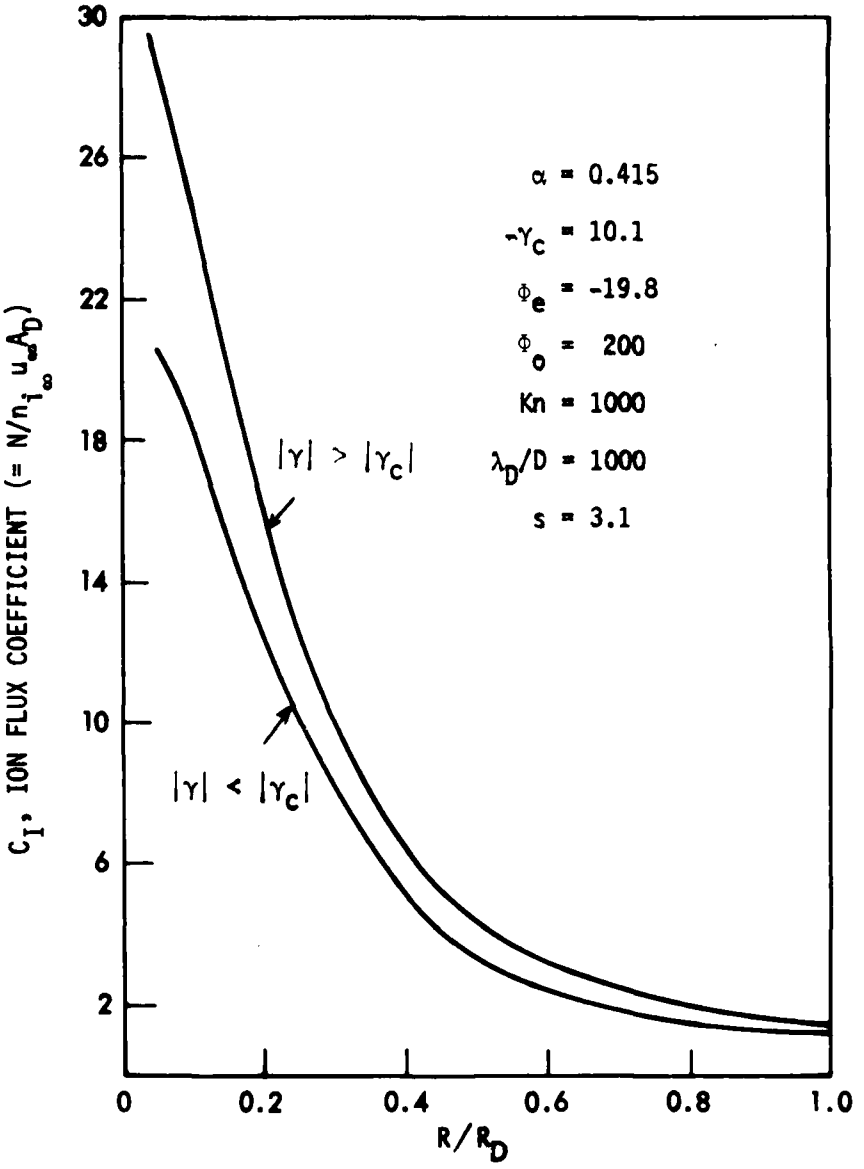

FIG. 9. ION FLUX DISTRIBUTION AS FUNCTION OF RADIUS FOR $\alpha = 0.415$

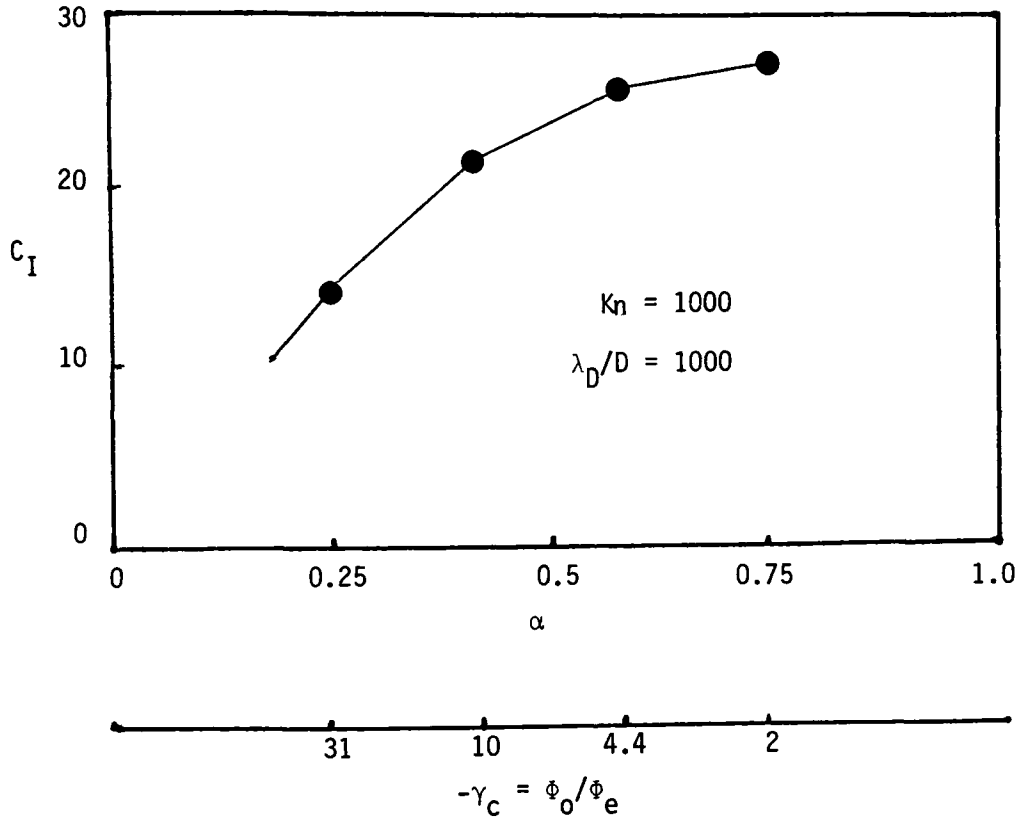

FIG. 10. STAGNATION POINT ION FLUX COEFFICIENT AS FUNCTION OF α FOR $\gamma = \gamma_c$

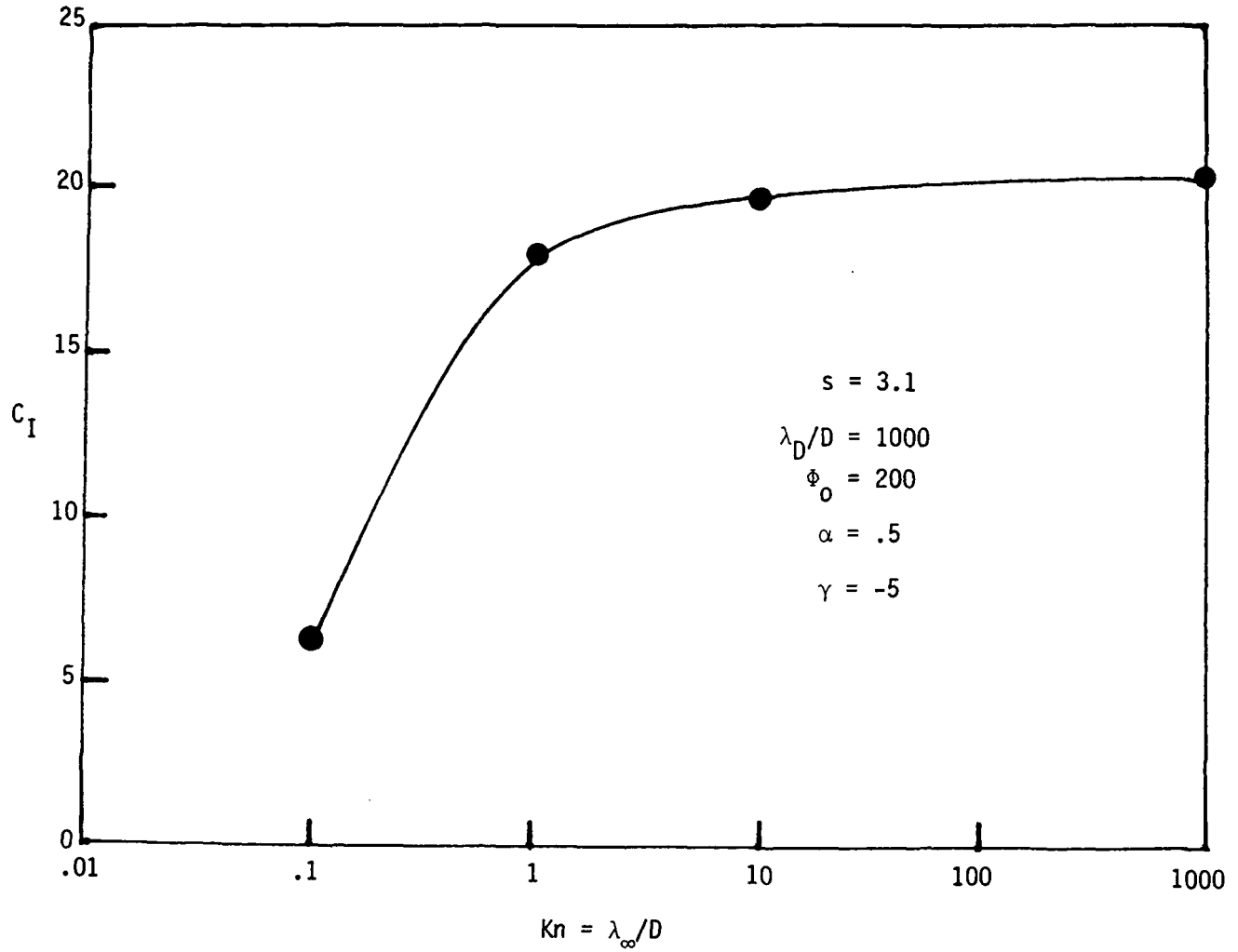

FIG. 11. STAGNATION-POINT ION FLUX VARIATION WITH KNUDSEN NUMBER

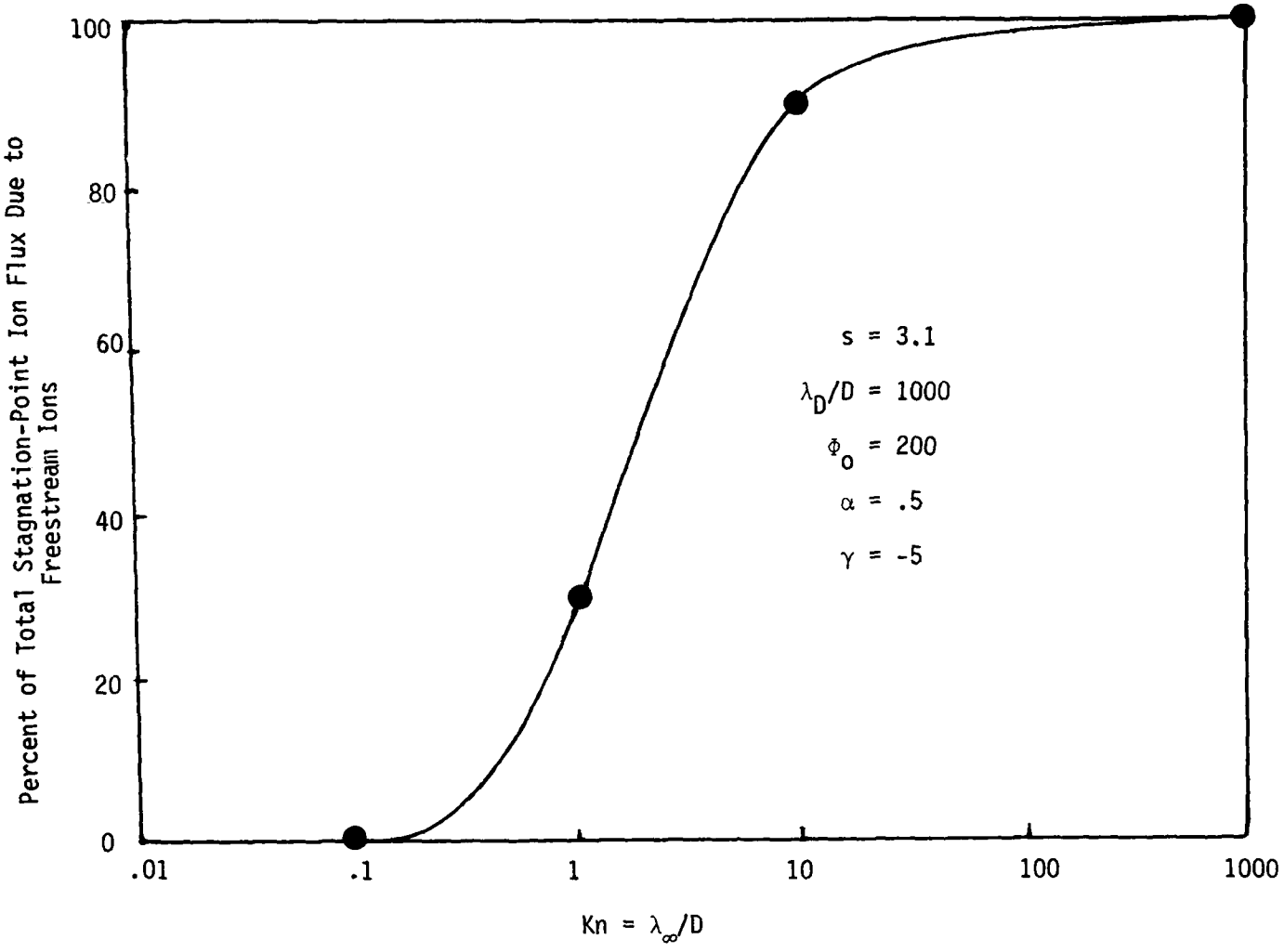

FIG. 12. FRACTION OF FREESTREAM IONS IN STAGNATION-POINT FLUX

This behavior of the negative-ion collection probe is not unlike its behavior when positive ions are collected. A direct comparison of the stagnaton-pointion flux coefficients is given in Figure 13 for the parameters indicated. In both cases the effect of collisions starts to appear at a Knudsen number of about 10. Note that the stagnation-point flux for the negative ions is substantially higher at large Knudsen numbers than that for positive ions because of the strong focussing effect of the double-disk configuration (whereas for positive-ion collection the flux is much more uniform across the face of the probe). At Knudsen numbers less than unity, this focussing is greatly attenuated by collisions. An additional comparison between negative and positive ion collection is shown in Figure 14 where the fraction of freestream ions in the stagnation-point flux is plotted versus Knudsen number.

4.3 FLUX VARIATION WITH DEBYE NUMBER

The simulations for various Debye numbers were performed with a Knudsen number of 1000 and the other parameters set as before. The results of these calculations are summarized in Figure 15 where the stagnation-point flux of negative ions is plotted versus Debye number. The variation with Debye number is qualitatively similar to the results for positive-ion collection except that the roll-off in the flux with decreasing Debye number appears to be more gradual for negative-ion collection. Note that results could not be obtained for Debye numbers less than 0.1 due to instabilities in the Poisson solution and in fact the result at De = 0.1 may be in error.

One observation that applies to the complete range of Knudsen and Debye numbers investigated is that there is no flux of positive ions to the stagnation point.

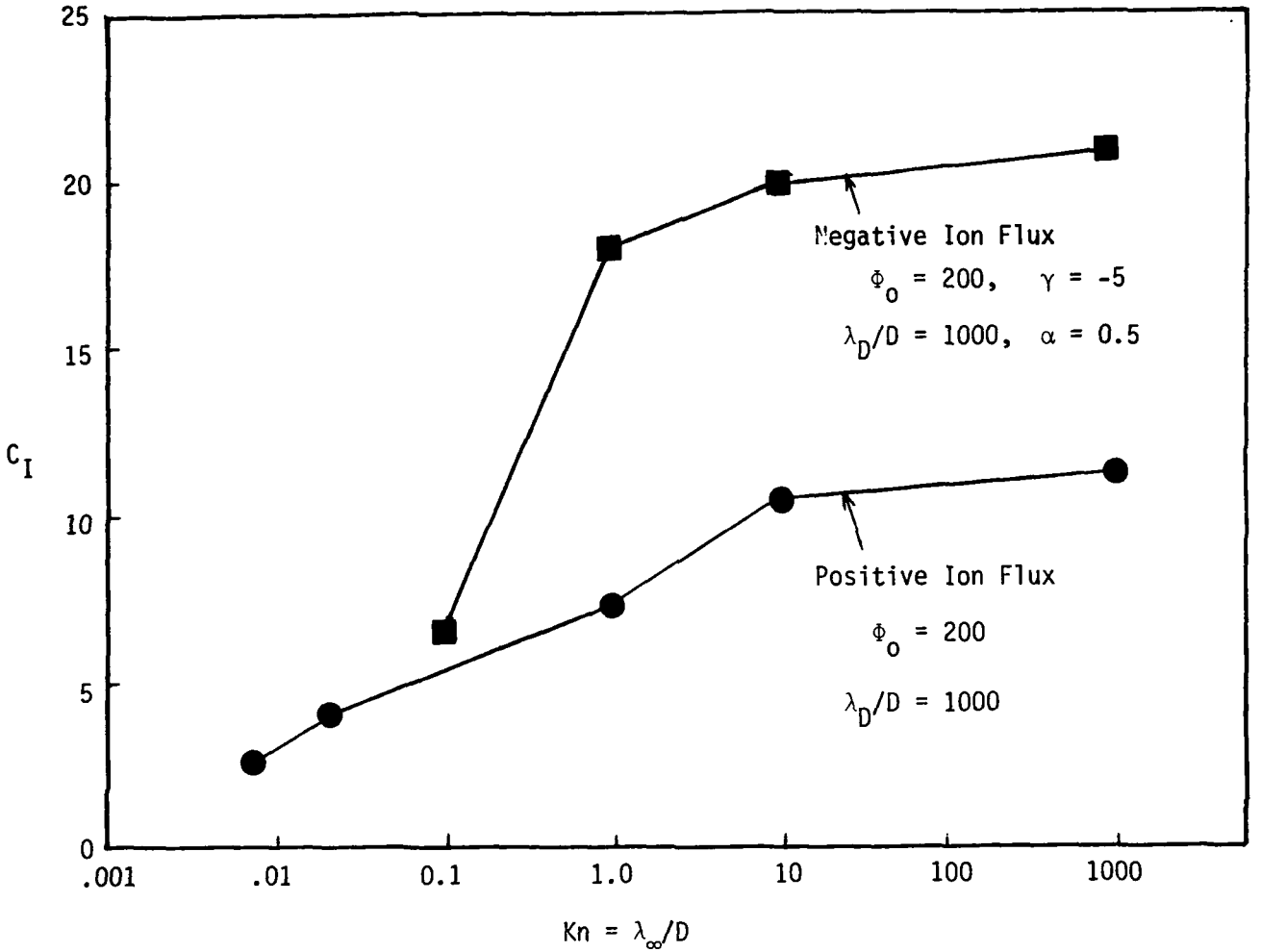

FIG. 13. STAGNATION POINT ION FLUX COEFFICIENT COMPARISONS AS FUNCTION OF KNUDSEN NUMBER

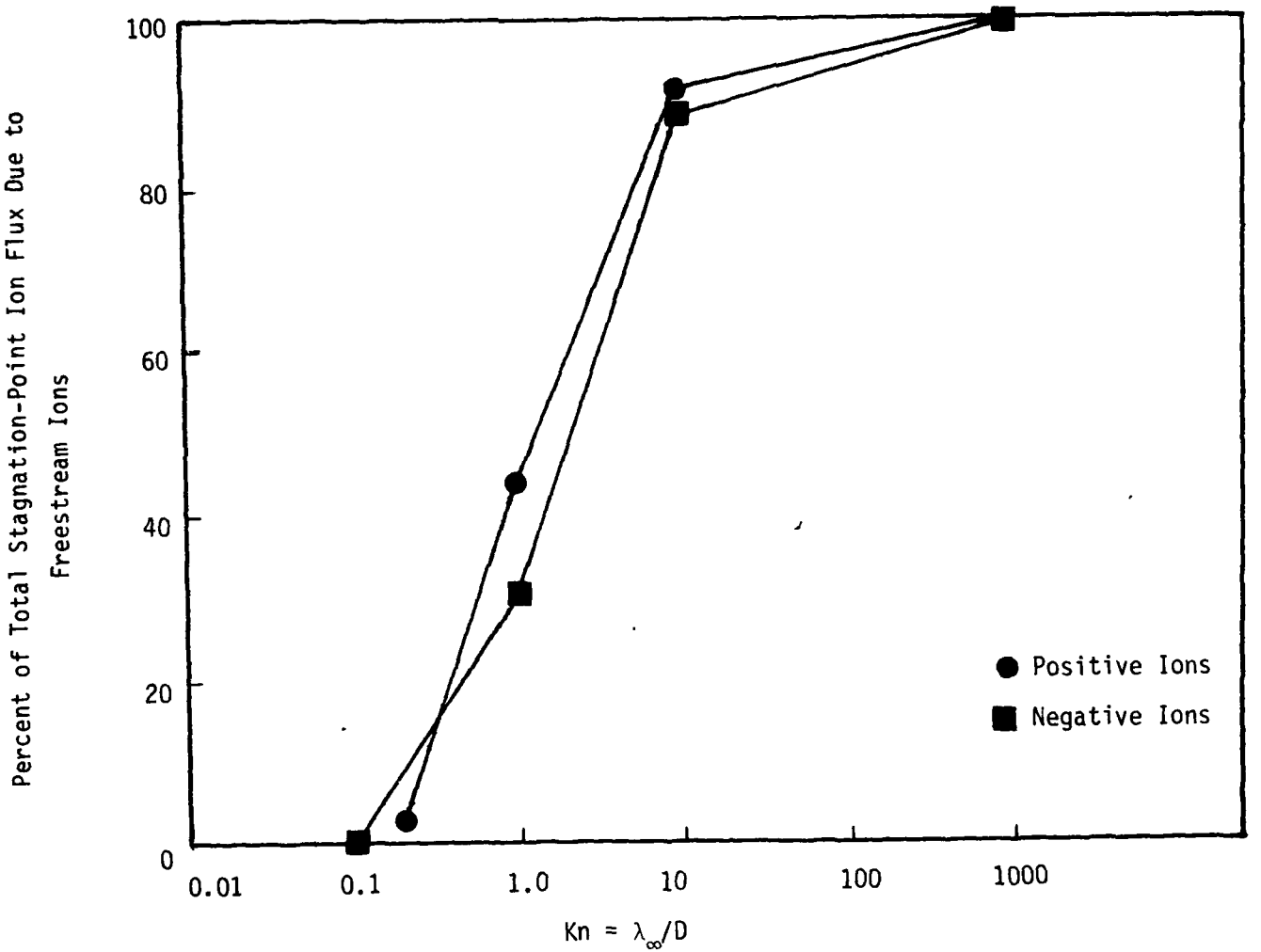

FIG. 14. FRACTION OF FREESTREAM IONS IN STAGNATION POINT FLUX

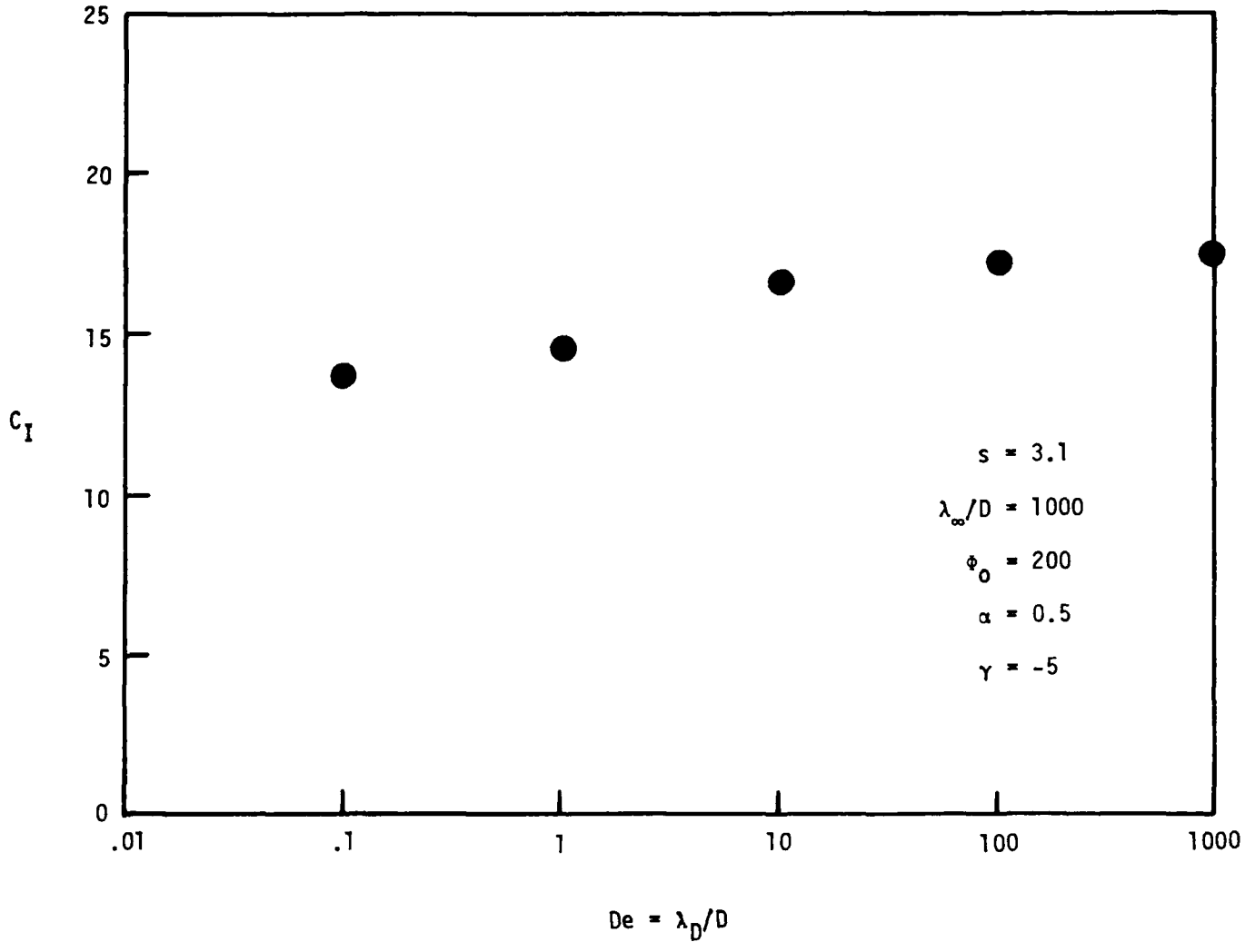

FIGURE 15. STAGNATION-POINT ION FLUX VARIATION WITH DEBYE NUMBER

5. SIMULATION OF IONOSPHERIC CHEMISTRY

5.1 INTRODUCTION

Collision theory is well established as an elementary classical theory for bimolecular gas reactions, and the concepts are readily incorporated in the direct simulation method. It is a phenomenological approach in that the binary reaction rate is obtained as the product of the kinetic theory collision rate for collisions with energy in excess of the activation energy and the probability of reaction or steric factor P_r. The steric factor may be regarded as the ratio of the reactive cross-section to the total collision cross-section and is inferred from a comparison of the theoretical prediction with the measured reaction rate. The simplest theory (for example[1]) employs a constant steric factor and considers only the translational collision energy in relation to the activation energy. Refinements of the method employ a collision energy dependent steric factor and allow for the possible contribution of the internal energy of the molecules in the collision. Collision theory may also be extended to termolecular reactions (for example[2]) by assigning a lifetime to each binary collision and regarding the triple or ternary collision as a further binary collision between the pair of molecules in the initial collision and a third molecule.

The reaction of most obvious interest in an aerodynamic context is the dissociation-recombination of oxygen and nitrogen. These are bimolecular reactions with finite activation energies for dissociation and termolecular reactions for recombination. The direct-simulation method was applied to this reaction by Bird.[3] These calculations employed a constant steric factor and the results for the dissociation rate were in agreement with the theoretical prediction. Also, the density and temperature dependence of the equilibrium state was in agreement with the law of mass action for this reaction.[4] The gas model was, however, unrepresentative of a real diatomic gas in that there was no internal energy. A further difficulty was that computing time considerations ruled out calculations at temperatures small compared with the characteristic dissociation temperature. Similar calculations which include the effects of internal energy modes have recently been made by Larsen.[5]

Bird[6] developed a collision theory analysis of the dissociation-recombination reaction to produce an expression for the equilibrium state that is identical in form to the law of mass action. If a particular diatomic gas is to be simulated, a comprison of the theoretical and experimental dissociation rates gives the appropriate steric factor, while a comparison of the theoretical and experimental values for the equilibrium degree of dissociation provides the binary collision lifetime parameter. The model corresponding to this extended theory was combined with Borngakke and Larsen's model[7] for the internal energy modes and was used to compute the dissociation relaxation zone behind a strong shock wave in nitrogen.[8] The ability to calculate the equilibrium state was particularly valuable in setting up the boundary conditions for the shock wave simulation. The simulation results were in good agreement with corresponding experimental results.

A difficulty that was encountered in the nitrogen simulation was that the negative temperature exponent in the rate equation was below the lower limit allowed in the theory. This had to be allowed for by a temperature, as well as collision energy, dependence of the steric factor. The following section presents a further extension of the bimolecular theory to include the contribution of the internal energy modes. As well as being more general, it allows much larger negative temperature exponents in the rate equations and would have coped with the accepted value for nitrogen. Unlike the existing collision theory based on the "effective square term" approach[1,3], it is not restricted to temperatures that are small in comparison with the characteristic temperature of the reaction. A further extension is that the model now deals with inverse power law molecules rather than being restricted to hard sphere molecules. The wider applicability of the new model is particularly useful when dealing with cases which involve a very large number of reactions.

5.2 DERIVATION OF STERIC FACTORS FROM REACTION RATES

A typical bimolecular reaction may be written

$$A + B \rightleftharpoons C + D \,, \qquad (1)$$

where A, B, C, and D represent separate molecular species. The rate equation for species A may be written

$$-\frac{dnA}{dt} = k_f(T)\, n_A n_B - k_r(T)\, n_C n_D \,. \qquad (2)$$

where n is the number density with the subscripts representing the species, t is the time and $k_f(T)$ and $k_r(T)$ are the forward and reverse rate coefficients. The temperature T dependence of the rate coefficient is generally of the form

$$k(T) = a\, T^b \exp(-Ea/kT) \,, \qquad (3)$$

where a and b are constants, Ea is the activation energy, and k is the Boltzmann constant. The problem is to find an expression for the steric factor, or collision probability, Pr as a function of the collision energy E_c that leads explicitly to Eq. (3) in the context of collision theory.

The collision energy E_c is equal to the sum of the relative translational energy in the collision and the fraction internal energy of the two molecules that may contribute to the reaction. The translational energy is equal to $1/2\, m_r c_r^2$ where $m_r = m_1 m_2/(m_1 + m_2)$ is the reduced mass and c_r is the relative speed. The internal energy is best dealt with by specifying that the number of degrees of freedom of the two molecules that may contribute energy to the reaction is ζ_1 and ζ_2. This number may range from zero to the number of degrees of the molecule, although there are restrictions based on angular momentum considerations on the number of rotational degrees of freedom that can be active in a reaction.[9] It is readily shown that, for an equilibrium gas, the distribution function of E_c/kT is

$$f\left(\frac{E_c}{kT}\right) = \frac{1}{\Gamma\left(\frac{\zeta_1+\zeta_2}{2} + \frac{\eta-3}{\eta-1} + 1\right)} \left(\frac{E_c}{kT}\right)^{\frac{\zeta_1+\zeta_2}{2}+\frac{\eta-3}{\eta-1}} \exp\left(-\frac{E_c}{kT}\right) , \qquad (4)$$

where η is the exponent of inverse power law intermolecular force and Γ is the Gamma function. Collision theory assumes that the forward rate equation is given by

$$\frac{dn_A}{dt} = - n_A \nu_{AB} \int_{\frac{E_a}{kT}}^{\infty} f\left(\frac{E_c}{kT}\right) P_r d\left(\frac{E_c}{kT}\right) , \tag{5}$$

where ν_{AB} is the equilibrium collision rate for a species A molecule with species B molecules, and E_A is the activation energy such that the reaction probability is zero for E_c less than E_a. Now

$$\nu_{AB} = n_B \overline{\sigma_T c_r} ,$$

where σ_T is the total collision cross-section and the bar denotes the mean value. A comparison of Eqs. (2) and (5) then shows that

$$k(T) = \overline{\sigma_T c_r} \int_{\frac{E_a}{kT}}^{\infty} f\left(\frac{E_c}{kT}\right) P_r d\left(\frac{E_c}{kT}\right) . \tag{6}$$

For hard sphere ($\eta = \infty$) molecules, the standard result is that

$$\overline{\sigma_T c_r} = (d_1 + d_2)^2 \left(\frac{\pi kT}{2m_r}\right)^{1/2} \tag{7}$$

where d is the molecular diameter while, for general values of η,

$$\overline{\sigma_T c_r} = W_{Om}^{\ 2} (K/m_r)^{\frac{2}{\eta-1}} c_r^{\frac{\eta-5}{\eta-1}} , \tag{8}$$

where W_{Om} is the cut-off value of the dimensionless impact parameter and K is the constant in the force law. The parameter W_{Om} is related to the lower cut-off value that must be chosen for the deflection angle in the collision. The value of P_r will depend on this choice and the generalized collision theory is unsatisfactory when the overall aim is merely the

calculation of the steric factor P_r. However, this is not a difficulty when this factor is used in the direct simulation method since a cut-off value must be specified anyway.

If a constant steric factor is employed in Eq. (6), it may be taken outside the integration which then yields

$$\Gamma\left(\frac{\zeta_1 + \zeta_2}{2} + \frac{\eta - 3}{\eta - 1} + 1, \frac{E_a}{kT}\right) \Big/ \Gamma\left(\frac{\zeta_1 + \zeta_2}{2} + \frac{\eta - 3}{\eta - 1} + 1\right) .$$

For integer values of the first argument, the incomplete Gamma function may be written as a power series in E_a/kT. This is effectively done in the "activation in many degrees of freedom" theory[1] and the "square term" theory.[4] All but the leading term of the power series may be discarded when $kT \ll E_a$ but, while this is satisfactory for the dissociation-recombination reaction, it is out of the question for fast exothermic reactions. This problem may be avoided by the introduction of a steric factor proportional to some power of $E_c - E_a$ multiplied by the term

$$\left(1 - \frac{E_a}{E_c}\right)^{\frac{\zeta_1 + \zeta_2}{2} + \frac{\eta - 3}{\eta - 1}} .$$

This term enables the incomplete Gamma function to be transformed to a Gamma function that does not involve the temperature, and leads to the desired form of Eq. (3) for k(T). Moreover, this modification has physical as well as mathematical advantages. It means that P_r need no longer be constant for very large values of E_c and the rise from zero at $E_c = E_a$ is no longer discontinuous. Similar forms for the steric factor have, in fact, been proposed for these reasons.[1,10]

The full expression for the steric factor that yields Eq. (3) when substituted into Eq. (6) with Eqs. (4) and (8) is

$$P_r = \frac{\varepsilon}{2\pi\, \tfrac{1}{2} W_{0m}^{\,2}\, (k/m_e)^{\frac{2}{\eta-1}}} \frac{\Gamma\left(\frac{\zeta_1+\zeta_2}{2} + \frac{\eta-3}{\eta-1} + 1\right)}{\Gamma[2(\eta-2)/(\eta-1)]} \left(\frac{m_r}{2K}\right)^{\frac{\eta-5}{2(\eta-1)}} \frac{a}{\Gamma\left(\frac{\zeta_1\zeta_2}{2} + \frac{3}{2} + b\right)}$$

$$\cdot \left(1 - \frac{E_a}{E_c}\right)^{\frac{\zeta_1+\zeta_2}{2} + \frac{\eta-3}{\eta-1}} \left(\frac{E_c - E_a}{k}\right)^{b - \frac{\eta-5}{2(\eta-1)}} \tag{9}$$

The symmetry factor ε is equal to 1 for unlike molecules and 2 when both collision partners are of the same species. The use of Eq. (7) in place of Eq. (8) gives the following simplified form of Eq. (9) for hard sphere molecules:

$$P_r = \frac{\Gamma\left(\frac{\zeta_1+\zeta_2}{2} + 2\right)}{(d_1 + d_2)^2} \left(\frac{2m_r}{\pi k}\right)^{1/2} \frac{a}{\Gamma\left(\frac{\zeta_1+\zeta_2}{2} + \frac{3}{2} + b\right)} \left(1 - \frac{E_a}{E_c}\right)^{\frac{\zeta_1+\zeta_2}{2}+1} \left(\frac{E_c - E_a}{k}\right)^{b-1/2} \tag{10}$$

The minimum value of b is now $-\left(\frac{\zeta_1+\zeta_2}{2} + \frac{3}{2}\right)$ rather than the $-\frac{3}{2}$ allowed by earlier theory which does not take into account the contribution of the internal energy modes. The extended theory would have covered the experimental values for nitrogen that caused difficulties in the shock wave calculations.[8] This general behavior is consistent with the more restricted "square term" theory, in that increasing negative value of b are associated with a greater contribution from the internal degrees of freedom.

The use of Eqs. (9) or (10) to obtain the steric factor for use in a simulation program ensures that the reaction rates will agree with those from the continuum rate equation in flow situations where near translational and rotational equilibrium prevail and both the discrete particle and the continuum approaches are applicable. The discrete particle approach, through the direct-simulation method, permits results to be obtained for chemically reacting flow situations with marked non-equilibrium in the translational and internal modes. The critical question is the

degree of realism in the modeling of the real flow in this regime. It should be kept in mind that the above equations for the collision probability constitute phenomenological models which are not unique and which have been based largely on considerations of mathematical tractability. The ideal would be to have tabulations of reaction cross-sections as functions of the energy states and impact parameters based on quantum calculations and experiment. The progress in this direction has been reviewed by Toennies,[11] and very little of this information is currently available for reactions of engineering interest. When a classical approach based primarily on continuum rate data must be used, the above model appears to offer the most practical approach for chemically reacting flows in the transition regime. Hopefully, the physical basis is sufficiently sound for the predictions to be at least qualitatively valid.

In order to consider the direct simulation method as an alternative to conventional continuum calculations, the following conditions should be assessed.

The advantages are:

- The gas need not be in an equilibrium or quasi-equilibrium state. Not only may each species have a separate temperature, but the velocity distributions functions may vary drastically from the Maxwellian distribution and the internal modes may be out of equilibrium with the translational mode.

- The calculations make direct use of the reactive cross-sections as functions of the molecular properties and collision impact parameters. The fact that these do not have to be averaged to give rate constants as a function of temperature is particularly advantageous for electron-neutral and electron-ion reactions for which the cross-section versus energy curves often have closely spaced peaks and valleys. The vibrational states may be regarded as reactions. Radiative reactions may also be included.

The disadvantages are:

- The number of representative simulated modules is generally restricted to some thousands and the total number of simulated collisions to some millions. This means that it is impractical to simulate reactions which occur less frequently than once every thousand elastic collisons (i.e., steric factors less than about 10^{-3}). This rules out some very slow bimolecular reactions and generally rules out termolecular reactions.

- There are sampling difficulties associated with trace species, although these may be alleviated, to some extent, through the use of weighting factors such that the number of real molecules represented by each simulated molecule varies from species to species.

- Most of the currently available data is presented as rate coefficients as a function of temperature, rather than as reactive cross-sections as a function of the collision energy. This data must be analytically converted to give the same answer in the quasi-equilibrium situations for which the continuum approach is valid. (The magnitude of the steric factors given by this conversion process provides a useful check on the physical validity of the rate data.)

The above considerations lead to the conclusion that direct molecular simulation is most suitable for rapidly varying transient phenomena in the upper regions of the atmosphere. It can be used in situations where the conventional continuum approach would be invalid.

Illustrative Example

The direct simulation method has been applied to the vibrational excitation of steam. The reason for choosing steam is that it has[12] an anomalously rapid vibrational relaxation rate for V-T collisions. The scatter in the data is such that the temperature exponent is uncertain and a constant value of $3.5 \times 10^{-17} m^3 s^{-1}$ per molecule has been used for the deactivation rate. The characteristic temperature of the reaction is 2293K so that the activation rate coefficient given by the product of the deactivation coefficient and exp (-2295/T). The resulting steric factors from Eq. (10) are shown in Figure 16.

A homogeneous relaxation case was computed for initial conditions of T = 650K, $n = 10^{23} m^{-3}$ and n* = 0. Here, n and n* are the number densities of the ground state and first vibrational level, respectively. Eq. (2) becomes

$$\frac{d}{dt}\left(\frac{n^*}{n}\right) = 3.5 \times 10^6 \left[\exp - \left(\frac{2295}{T}\right) - \frac{n^*}{n}\right] \qquad (11)$$

and energy conservation requires,

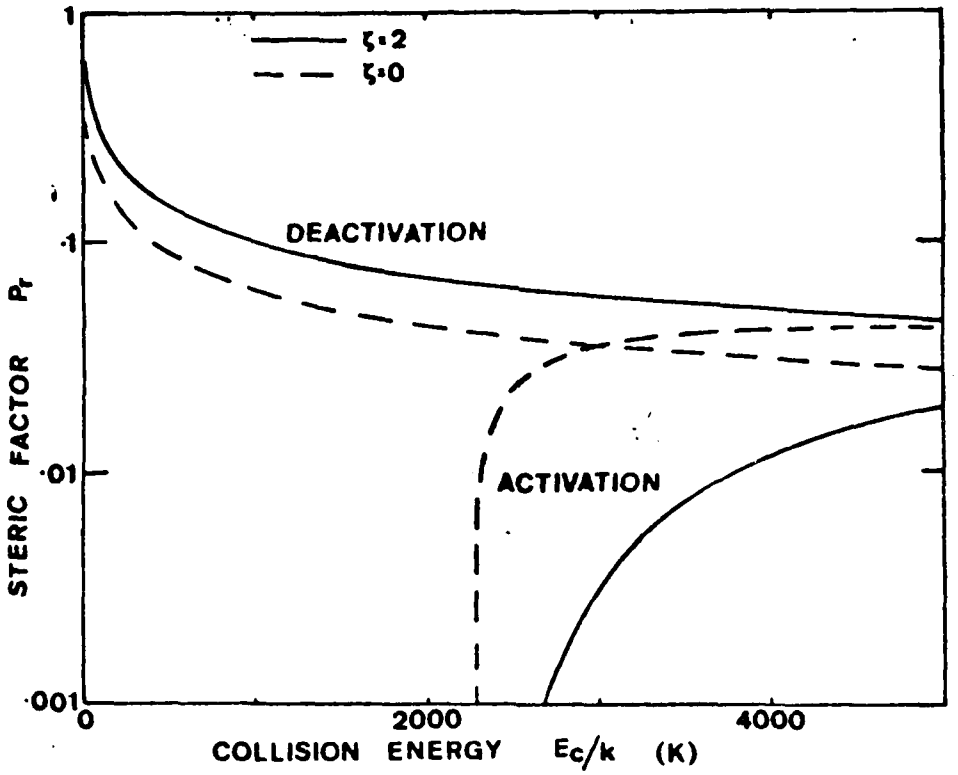

Figure 16. Steric factors for the activation and deactivation of the first vibrational level in steam.

$$T = 650 - 918\,(n^*/n)\ . \qquad (12)$$

Figure 17 compares the simulation results with a numerical solution of eqs. (11) and (12). The two are in good agreement even though this is a sufficiently fast reaction for a substantial departure from local translational and rotational equilibrium to be expected. The equilibrium concentration ratio is also in good agreement with the equilibrium value even though the simulation procedures based on collision theory cannot be expected to satisfy detailed balancing.

In order to illustrate the effects of translational equilibrium in a transition regime flow, the steam model was then applied to the steady flow through a screen or grid. This flow is schematically represented in Figure 18 which also defines the flowfield dimensions and the initial and boundary conditions. This is a one-dimensional flow in which the grid is a hypothetical device which reflects a specified percentage of the molecules passing through it. The initial temperature was chosen such that the initial equilibrium excitation is negligible and the grid solidity is sufficiently large to produce a temperature with a significant degree of equilibrium excitation. The temperature profiles along this flow ahead of the grid shown in Figure 19 are very similar to those for a normal shock wave. There is a temperature jump at the grid location and, since the downstream Mach number in this flow is barely supersonic, there is some upstream influence from the open end. The parallel temperature T_x based on the velocity components in the flow direction overshoots the overall temperature T by a significant margin. The normal temperature T_n based on the other components overshoots T by a small margin, while the rotational temperature T_r lags behind T.

Figure 20 compares the simulation results for the density ratio $n^*/(n + n^*)$ with those obtained from the solution of eq. (11) using the values of stream velocity, density and overall temperature given by the simulation. The non-equilibrium efffects are significant and, as would be expected from the temperature profiles in Fig. 19, they are greater when the collision energy E_c is obtained from the translational modes only. Other calculations showed that the vibrational overshoot is much larger

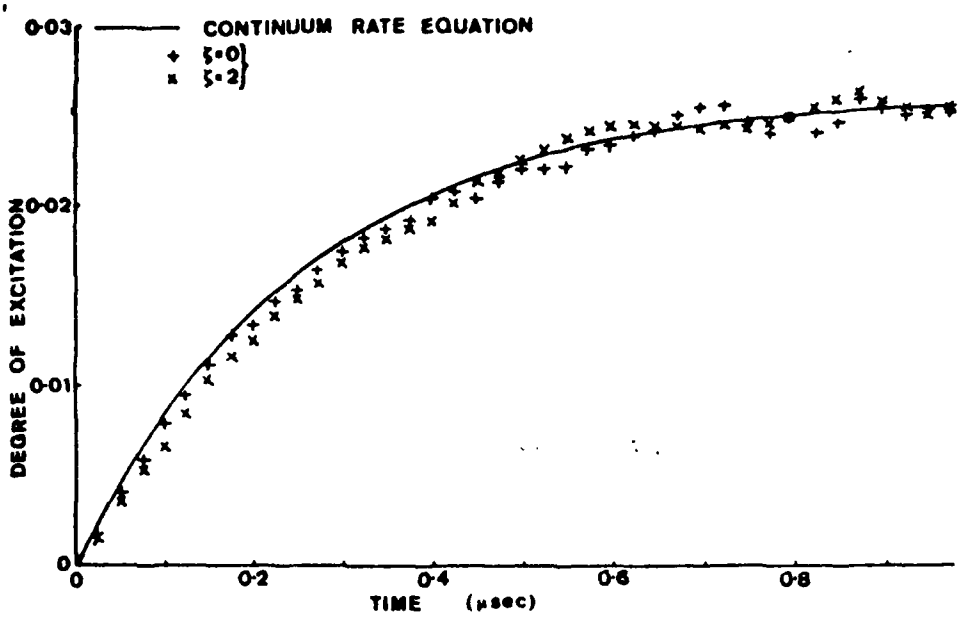

Figure 17. A comparison of the actual and simulation results for vibrational relaxation in steam.

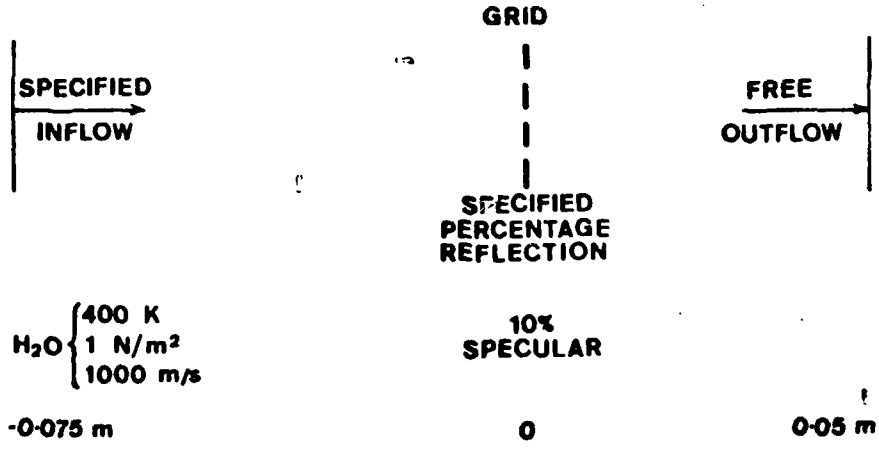

Figure 18. A schematic representation and data definition of the test case for the flow of steam through a grid.

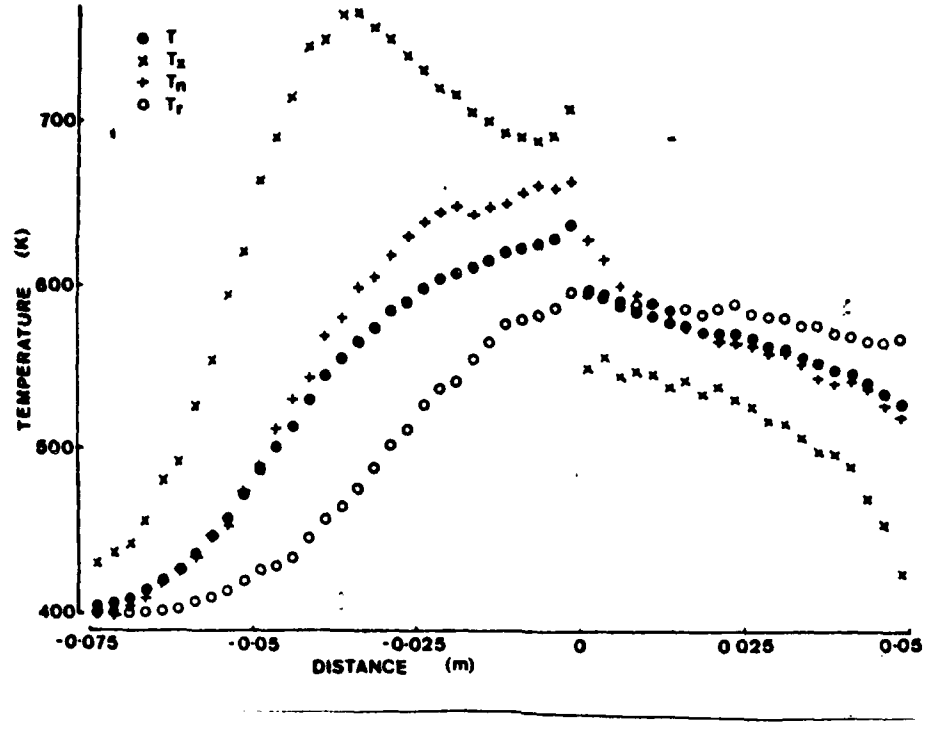

Figure 19. Temperature profiles for the flow of steam through a grid.

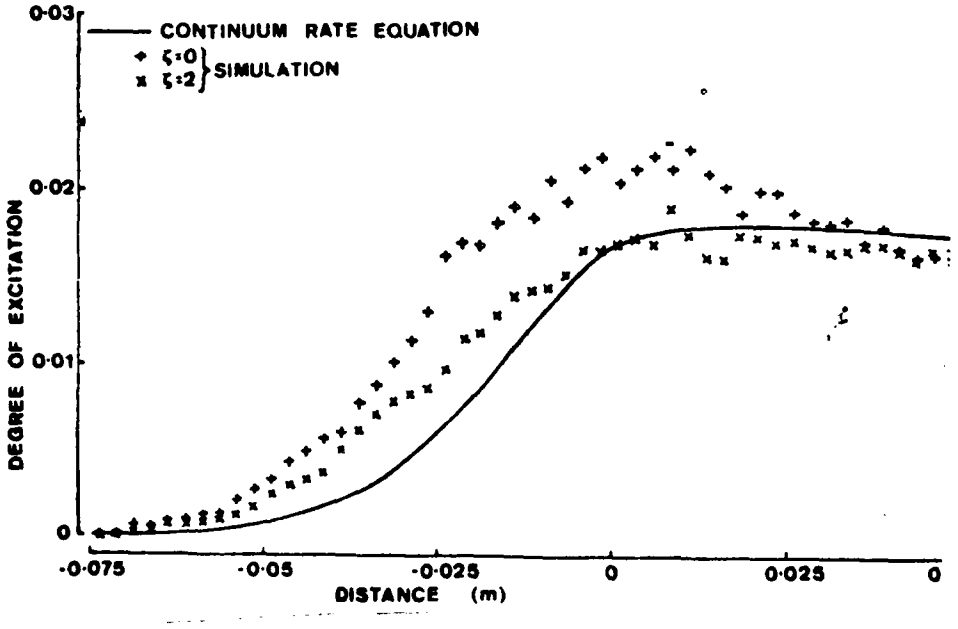

Figure 20. Vibrational excitation profiles for the flow of steam through a grid.

if the rate coefficient is proportional to a finite positive power of temperature, but is not greatly affected by the replacement of the basic hard sphere model by an inverse ninth power law model.

The above example illustrates the scope of the direct-simulation method when chemical data is available only in the form of bulk reaction rates. Approximate quantum cross-section predictions are available for T-V reactions such as that for steam in the second example. The direct-simulation approach would also be particularly useful for the reverse task of deducing rate coefficients or even flowfields from these predictions in order to make comparisons with experiment.

5.3 NEGATIVE ION COMPOSITION IN THE IONOSPHERE

A set of chemical reactions representative of the important processes in the ionosphere has been investigated by the direct simulation Monte Carlo method described earlier. In this calculation, a homogeneous gas mixture initially containing electrons, atomic oxygen, molecular oxygen, and molecular nitrogen. Equation (10) is used to convert the temperature dependent rate coefficients given below to collision energy dependent steric factors.

		$k(cm^3/s)$
Formation:	$e + O_2 \rightarrow O^- + O$	$< 10^{-16}$ for $T < 2000°K$
	$e + O_2 + O_2 \rightarrow O_2^- + O_2$	$(1.4 \pm 2) \times 10^{-29}\left(\frac{300}{T}\right)\exp\left(\frac{-600}{T}\right)\left(\frac{cm^6}{s}\right)$ for $(195 < T < 600)$
Exchange:	$O^- + O_2 \rightarrow O + O_2^-$	$< 10^{-10}$
	$O_2^- + O \rightarrow O_2 + O^-$	$\lesssim 10^{-10}$
		$k(cm^3/s)$
Detachment:	$O^- + O \rightarrow O_2 + e$	$1.7 \pm 0.3 \times 10^{-10}$
	$O_2^- + O_2 \rightarrow O + O_2 + e$	$2.3 \times 10^{-9} \exp\left(\frac{-2600}{T_i}\right)$ for $T_i < 2000$

$$O_2^- + O \rightarrow O_3 + e \qquad 3.2 \times 10^{-10}$$

$$O_2^- + O_2 \rightarrow O_2 + O_2 + e \qquad (2.7 \pm .3) \times 10^{-10} \left(\frac{T}{300}\right)^{\frac{1}{2}} \exp\left(\frac{-5590}{T}\right)$$

$$\text{for } (375 < T < 600)$$

$$O_2^- + N_2 \rightarrow O_2 + N_2 + e \qquad (1.94 \pm .4) \times 10^{-12} \left(\frac{T}{300}\right)^{1.5} \exp\left(\frac{-9990}{T}\right)$$

$$\text{for } (375 < T < 600)$$

$$O^- + N_2 \rightarrow O + N_2 + e \qquad 3.4 \times 10^{-9} \exp\left(\frac{-2600}{T_i}\right)$$

Most of the rate coefficients were obtained from the DNA Reaction Rate Handbook (DNA.19484), March 1972.

Two formation reactions are considered. One of these

$$e + O_2 + O_2 \rightarrow O_2^- + O_2$$

is a termolecular reaction with a rate coefficient that indicates that it occurs only once every 10^7 binary O_2, O_2 collisions at a number density of 10^9 to 10^{10} cm^{-3}. The other reaction

$$e + O_2 \rightarrow O^- + O$$

is bimolecular but, being dissociative, has a high activation energy of approximately 3.6 eV. Above this energy, the steric factor is of the order of 0.2. The exchange and detachment reactions have steric factors, in the energy range of interest, that range from the order of 10^{-3} to unity.

The test case that has been chosen is an atmosphere with a number of 10^{10} cm^{-3} (approx. 200 km), with initial mole fractions of 0.08 electrons, 0.74 atomic oxygen, 0.14 molecular oxygen and 0.04 molecular nitrogen, and at a temperature of 2000°K. The energy of the electrons is instantaneously raised to 3.6 eV and the reactions are followed for 0.4 seconds.

The composition is shown in Figure 6 as a function of time. The mole fraction of O^- increases to almost 0.04 around 0.12 seconds and then decreases. The fraction of O_2^- continues to increase over the period of the calculation. Figure 7 shows the species temperature over the same period. They are still a way from equilibrium at the end of the calculation (but this is a comparatively short calculation). In Figure 8 the differences in the translational and internal temperatures shown as a function of time indicate the nonequilibrium effects of the internal degrees of freedom.

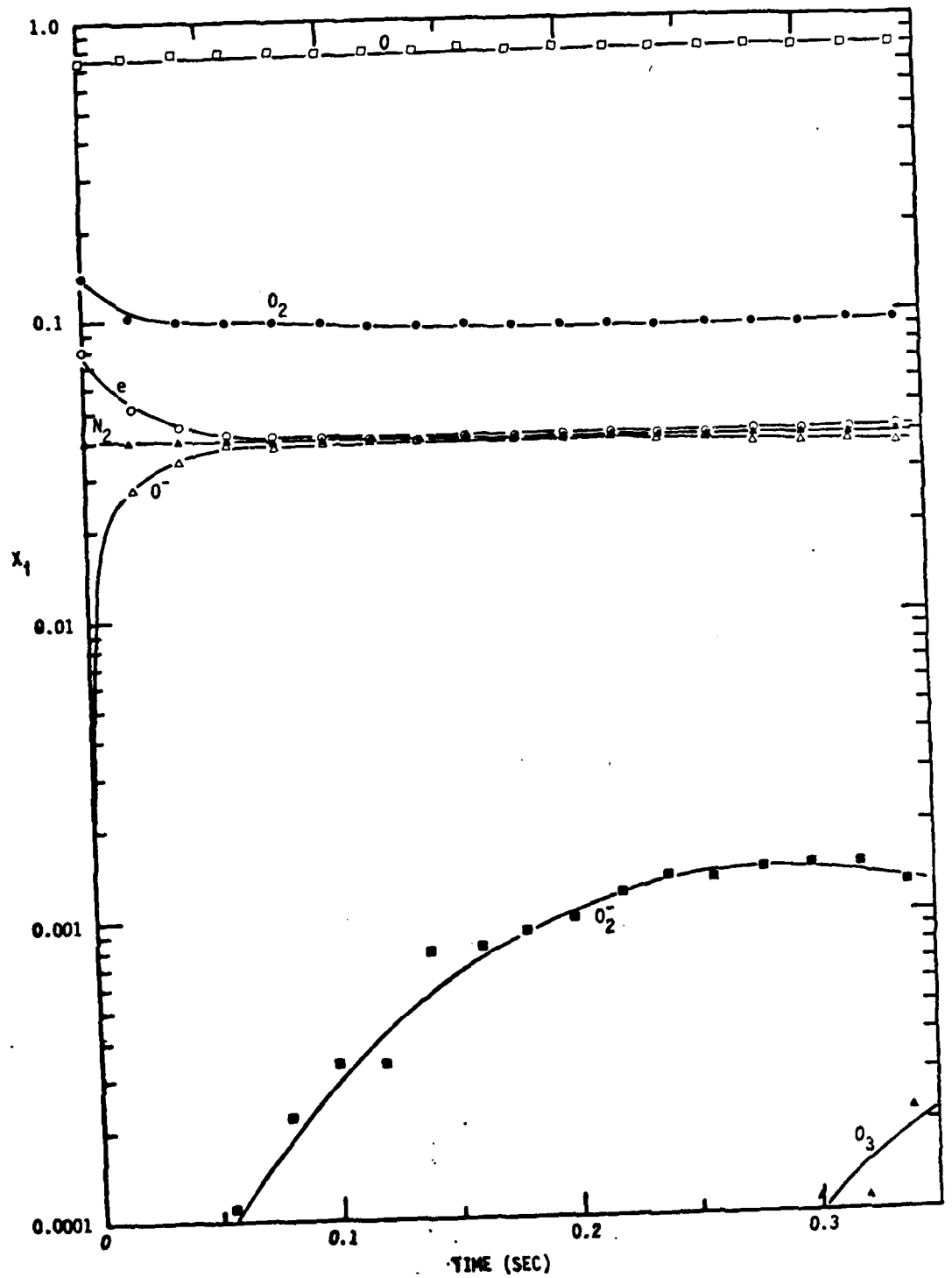

Figure 21. Mole fraction variation with time

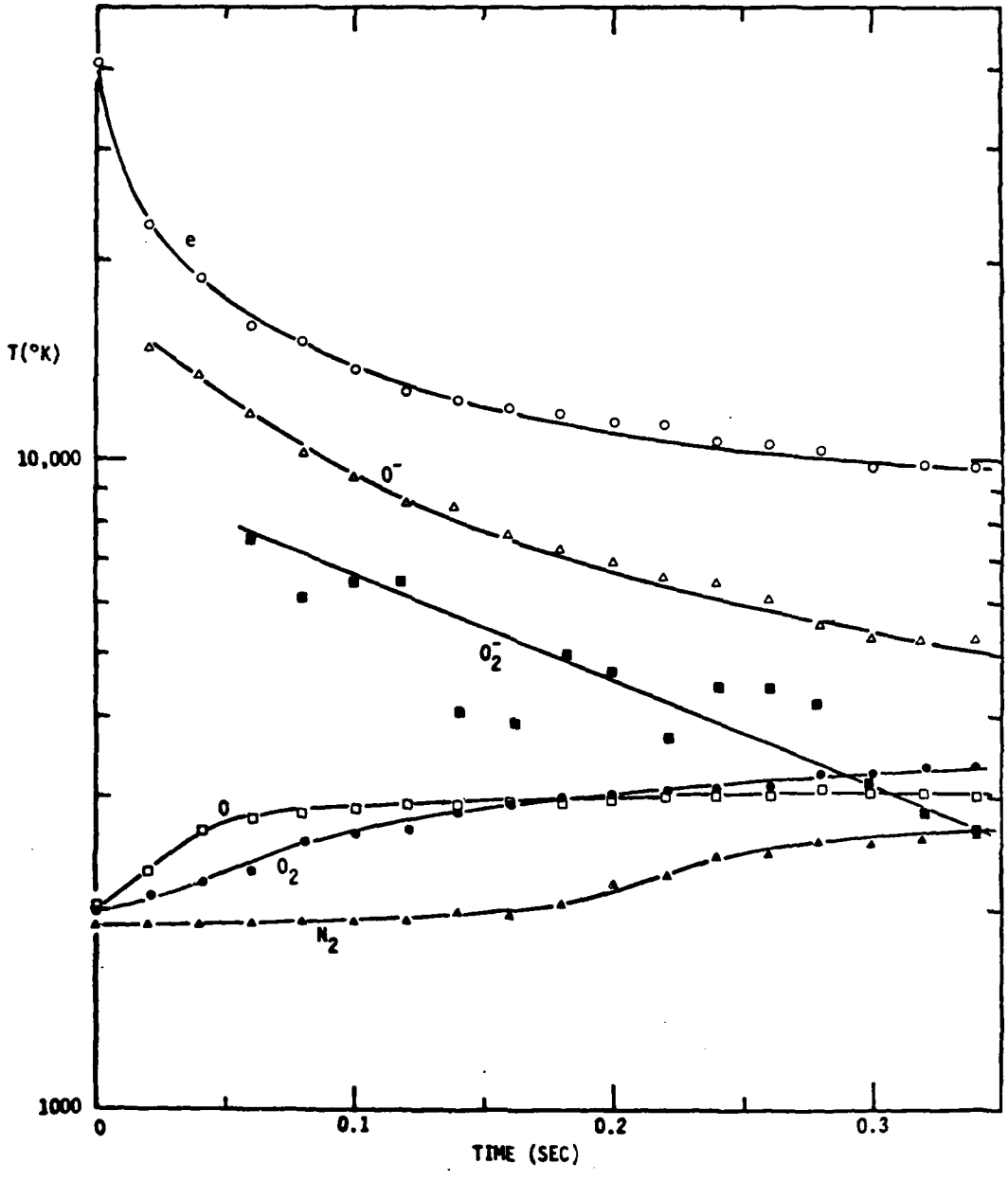

Figure 22. Translational temperature variation with time

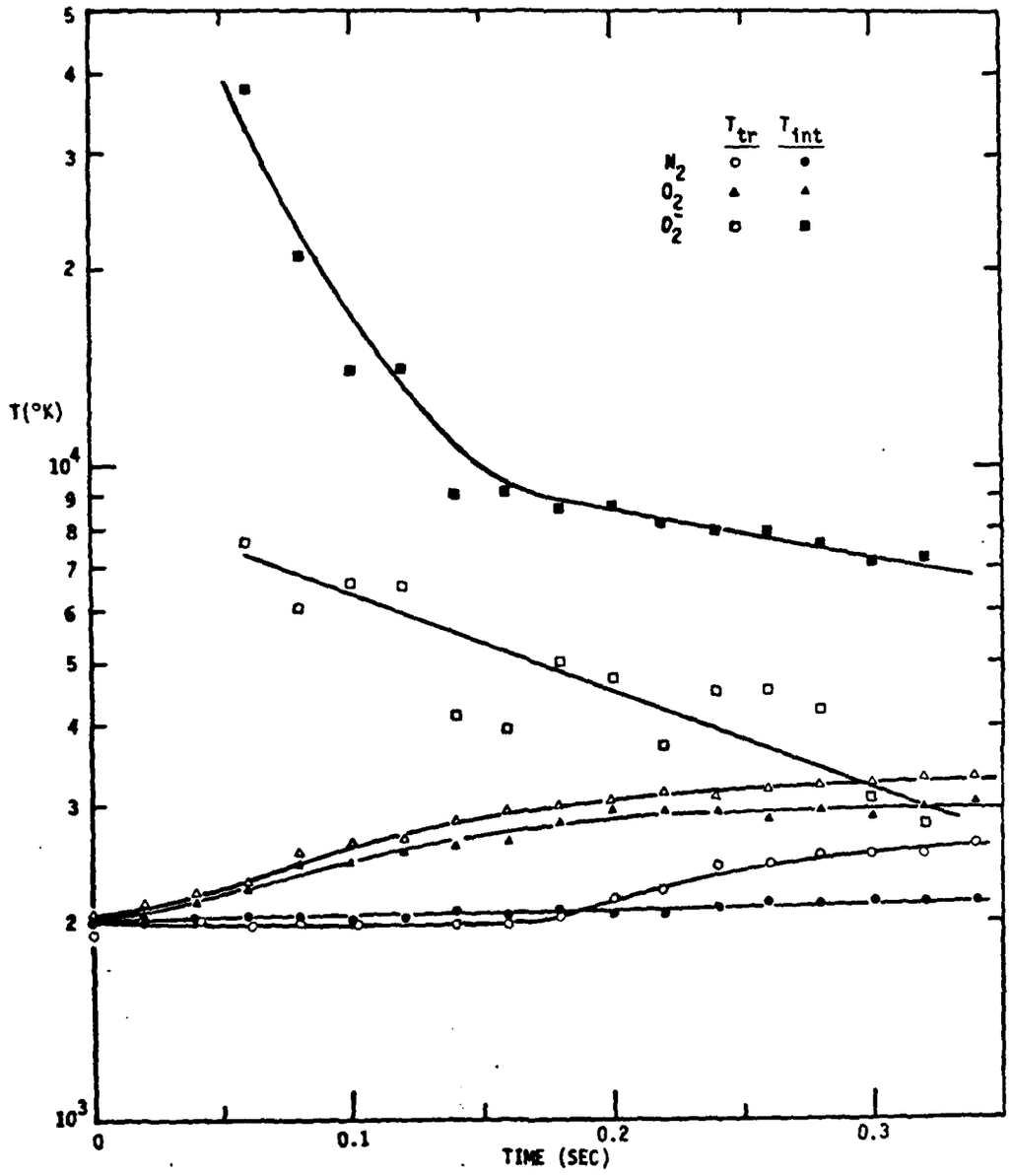

Figure 23. Translational (T_{tr}) and internal temperature (T_{int}) variation with time

6. CONCLUSIONS

The efforts to extend the direct simulation Monte Carlo method to the collection of negative ions have been shown to be more difficult than anticipated. As a result, it has been necessary to introduce a simplifying assumption for the behavior of the electrons at finite Debye numbers. Despite these difficulties, some useful results have been obtained. In particular, it has been found that realistic probe potentials (e.g., $\Phi_o = 200$, $\Phi_e = -40$, $\alpha = 0.5$) can produce a high stagnation-point flux of negative ions while completely rejecting positive ions. It was also discovered that this flux of negative ions is strongly attenuated by collisions at finite Knudsen numbers.

The application of the direct simulation Monte Carlo method to describe the chemistry in the ionosphere has been shown to be potentially a very useful computational tool. Although the calculations presented were restricted to a reaction cell simulation where there are no spatial gradients, the method does describe the effects of the electrons and ions and nonequilibrium influences which are not accounted for in the continuum descriptions. The procedure can be used to parametrically study the effect of high energy electrons on the chemistry of the ambient ionosphere or as a screening procedure for possible reaction chains. However, computational complexities prevented the incorporation of the chemistry simulation into the present ion collection code, although this remains as a possible activity for future work.

7. REFERENCES

1. Gardiner, W. C., Rates and Mechanisms of Chemical Reactions, (Benjamin, New York, 1969), Sections 4.2-3.

2. Smith, F. T., in Kinetic Processes in Gases and Plasmas, ed. by A. R. Hochstim, (Academic Press, New York, 1969), p. 257.

3. Bird, G. A., in Rarefied Gas Dynamics, ed. by D. Dine, (Editrice Technico Scientifica, Pisa, 1974), p. 693.

4. Vincenti, W. G. and Kruger, C. H., Introduction to Physical Gas Dynamics, (Wiley, New York, 1965), Chapter VII, Section 5.

5. Larsen, P. S., Archiv. of Mech., 28, 719 (1976).

6. Bird, G. A., Molecular Gas Dynamics, (Oxford Univ. Press, London, 1976), Chapter 12.

7. Borgnakke, C., and Larsen, P. S., J. Comput. Phys., 18, 405 (1975).

8. Bird, G. A., J. Comput. Phys., 25, 353 (1977).

9. See 4, p. 227.

10. Ross, J., Light, J. C., and Schuler, K. E., see Ref. 2, p. 281.

11. Toennies, J. P., in Rarefied Gas Dynamics, ed. by M. Becker and M. Fiebig, (DFVLR-Press, Porz-Wahn, 1974), Vol. 1, PAI-1.

12. Taylor, R. L., and Bitterman, S., Rev. Mod. Phys., 41, 26 (1969).

13. **Vogenitz, F. W., "Computer Simulation of Ion Collection by an Ionospheric Probe," TR-0006, Air Force Cambridge Research Lab., Bedford, Massachusetts, January 1973.**

14. **Sugimura, T. and Vogenitz, F. W., "Monte Carlo Simulation of Ion Collection by a Rocket Borne Mass Spectrometer for Collisionless and Transitional Flowfields," TR-73-0448, Air Force Cambridge Research Lab., Bedford, Massachusetts, July 1973.**

15. **Sugimura, T. and Vogenitz, F. W., "Monte Carlo Simulation of Ion Collection by a Rocket Borne Mass Spectrometer," Journal Geophysical Research, Vol. 80, No. 4, February 1975.**

16. **Sugimura, T., "Prediction of Positive Ion Collection by a Rocket Borne Mass Spectrometer," presented at 10th International Symposium on Rarefied Gas Dynamics, Aspen, Colorado, Paper No. 59, July 19-23, 1976 (to be published in the proceedings).**

17. **Sherman, C. and Parker, L. W., "Potential Due to a Circular Double Disk," AFCRL-70-0568, Air Force Cambridge Research Lab., Bedford, Massachusetts, 12 October 1970 (also Journal of Applied Physics, Vol. 42, No. 2, February 1971).**

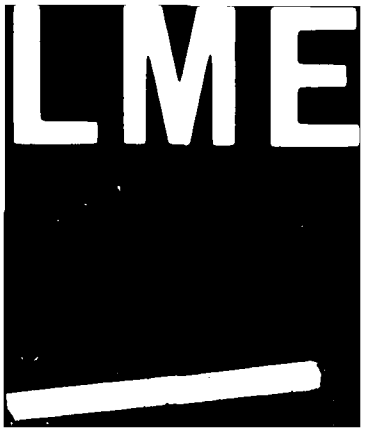
LME